Leptonic probes of Alternative Left-Right Symmetric Models

Mariana Frank,[1, *] Benjamin Fuks,[2, 3, †] Sumit K. Garg,[4, ‡]

Chayan Majumdar,[5, §] Poulose Poulose,[3, ¶] and Supriya Senapati[6, **]

[1]*Department of Physics, Concordia University,7141 Sherbrooke St. West, Montreal, QC H4B 1R6, Canada*
[2]*Laboratoire de Physique Théorique et Hautes Énergies (LPTHE), UMR 7589,*
Sorbonne Université & CNRS, 4 place Jussieu, 75252 Paris Cedex 05, France
[3]*Department of Physics, Indian Institute of Technology Guwahati, Assam 781 039, India*
[4]*Manipal Centre for Natural Sciences, Manipal Academy of Higher Education,*
Dr.T.M.A. Pai Planetarium Building, Manipal-576104, Karnataka, India
[5]*Department of Physics and Astronomy, University College London, London WC1E 6BT, United Kingdom*
[6]*Amherst Center for Fundamental Interactions, Department of Physics,*
University of Massachusetts, Amherst, MA 01003, USA

We explore constraints on the parameter space of the alternative left-right model originating from the leptonic sector. Our analyses focuses on both lepton-flavour-conserving observables, particularly the anomalous magnetic moment of the muon, and lepton-flavour-violating processes like $\mu \to e\gamma$ decay and $\mu - e$ conversions in nuclei. While contributions to the anomalous magnetic moment fall below the measured values at 2σ, current and future experimental sensitivities to flavour-violating branching rations of the Standard Model leptons are expected to impose lower bounds on the mass of the peculiar $SU(2)_R$ gauge boson of the model. This provides complementary constraints relative to existing limits, which are indirect and derived from collider bounds on the mass of the associated neutral gauge boson Z'.

I. INTRODUCTION

The Standard Model (SM) of particle physics, based on the gauge group $SU(3)_C \otimes SU(2)_L \otimes U(1)_Y$, successfully describes the properties of the elementary particles and their interactions. While its predictions match experimental data with remarkable accuracy, the SM faces several unresolved puzzles and conceptual challenges. Notably, it is a chiral framework, with maximal parity violation through the weak interaction, while the strong and electromagnetic interactions conserve parity. Additionally, the SM does not include right-handed neutrinos or extra fermionic states, preventing it from explaining observations from neutrino experiments which have firmly established that neutrinos are massive and they mix. Among the various theoretical frameworks proposed to extend the SM and address these issues, left-right symmetric models (LRSMs) [1–4] offer an attractive alternative. Based on the gauge group $SU(3)_C \otimes SU(2)_L \otimes SU(2)_R \otimes U(1)_{B-L}$, LRSMs relate the maximal breaking of parity to the smallness of the neutrino masses. By postulating parity invariance of weak interactions via interchangeable $SU(2)_L$ and $SU(2)_R$ symmetries, such frameworks automatically include three right-handed neutrinos needed for the implementation of seesaw mechanism to explain the smallness of the observed neutrino masses. Moreover, the $U(1)$ charge assignments are less arbitrary than in the SM, as the hypercharge quantum numbers now emerge from the mixing of the (gauged) $B - L$ symmetry and $SU(2)_R$, both having a physical origin.

The left-right symmetry can also be seen as emerging from a grand-unified framework based on the exceptional group E_6 [5–7], which is broken to its maximal subgroup $SU(3)_C \otimes SU(3)_L \otimes SU(3)_H$. The first of these $SU(3)$ factors remains unbroken and is identified with the SM strong interaction symmetry, while the other two are further broken down to $SU(2)_L \otimes SU(2)_H \otimes U(1)_X$ and then to the electroweak symmetry group. According to this structure, the fermions of the theory lie in $SU(3)_H$ triplets. There are three different ways to form an $SU(2)_H$ doublet from the three components of an $SU(3)_H$ triplet [8]. Canonical LRSM constructions identify $SU(2)_H$ with $SU(2)_R$, and impose that the first two components of the $SU(3)_H$ triplets are paired into $SU(2)_R$ doublets comprised of the right-handed SM fermions and neutrinos ν_R (which are singlets under the SM gauge symmetry). The symmetry breaking pattern requires an extended Higgs sector that features several scalar fields whose couplings to $SU(2)_L$ and $SU(2)_R$ doublets could yield unacceptably large tree-level flavour-changing neutral interactions. Consequently, conflicts with

---

*Electronic address: mariana.frank@concordia.ca
†Electronic address: fuks@lpthe.jussieu.fr
‡Electronic address: sumit.kumar@manipal.edu
§Electronic address: c.majumdar@ucl.ac.uk
¶Electronic address: poulose@iitg.ac.in
**Electronic address: ssenapati@umass.edu

Field	$\mathcal{G}_{\mathrm{ALRM}}$	$U(1)_S$	Field	$\mathcal{G}_{\mathrm{ALRM}}$	$U(1)_S$	Field	$\mathcal{G}_{\mathrm{ALRM}}$	$U(1)_S$
$\chi_L = \begin{pmatrix} \chi_L^+ \\ \chi_L^0 \end{pmatrix}$	$(\mathbf{1},\mathbf{2},\mathbf{1})_{\frac{1}{2}}$	0	$Q_L = \begin{pmatrix} u_L \\ d_L \end{pmatrix}$	$(\mathbf{3},\mathbf{2},\mathbf{1})_{\frac{1}{6}}$	0	$L_L = \begin{pmatrix} \nu_L \\ e_L \end{pmatrix}$	$(\mathbf{1},\mathbf{2},\mathbf{1})_{-\frac{1}{2}}$	1
$\chi_R = \begin{pmatrix} \chi_R^+ \\ \chi_R^0 \end{pmatrix}$	$(\mathbf{1},\mathbf{1},\mathbf{2})_{\frac{1}{2}}$	$\frac{1}{2}$	$Q_R = \begin{pmatrix} u_R \\ d_R' \end{pmatrix}$	$(\mathbf{3},\mathbf{1},\mathbf{2})_{\frac{1}{6}}$	$-\frac{1}{2}$	$L_R = \begin{pmatrix} n_R \\ e_R \end{pmatrix}$	$(\mathbf{1},\mathbf{1},\mathbf{2})_{-\frac{1}{2}}$	$\frac{3}{2}$
$\Phi = \begin{pmatrix} \phi_1^0 & \phi_2^+ \\ \phi_1^- & \phi_2^0 \end{pmatrix}$	$(\mathbf{1},\mathbf{2},\mathbf{2}^*)_0$	$-\frac{1}{2}$	d_L'	$(\mathbf{3},\mathbf{1},\mathbf{1})_{-\frac{1}{3}}$	-1	n_L	$(\mathbf{1},\mathbf{1},\mathbf{1})_0$	2
			d_R	$(\mathbf{3},\mathbf{1},\mathbf{1})_{-\frac{1}{3}}$	0	ν_R	$(\mathbf{1},\mathbf{1},\mathbf{1})_0$	1

TABLE I: ALRM scalar (left), quark (centre) and lepton (right) fields, their representation under $\mathcal{G}_{\mathrm{ALRM}}$, and their $U(1)_S$ charge assignments.

observations can only be avoided if the breaking of the $SU(2)_R$ symmetry occurs at a very high scale. As a result, the spectrum of new particles is pushed beyond the reach of current collider experiments, and the effects of the new states could only be observed indirectly through the study of rare phenomena.

Alternatively, the $SU(2)_H$ symmetry could be identified with another symmetry group, $SU(2)_{R'}$, such that the first and third components of $SU(3)_H$ triplets are paired into doublets. In contrast to conventional LRSM constructions, Alternative Left-Right Models (ALRMs) [8–12] impose the down-type quark d_R and neutrino ν_R fields to be $SU(2)_{R'}$ singlets, while the up-type quark u_R and charged lepton e_R fields are paired into $SU(2)_{R'}$ doublets with an exotic quark field d_R' and scotino field n_R, respectively. For parity invariance, the matter sector of the theory additionally includes exotic $SU(2)_L \otimes SU(2)_{R'}$ singlets, specifically the d_L' and n_L states [13]. These exotic matter states further allow the theory to include a phenomenologically viable dark matter candidate [14, 15], and naturally prevent it from yielding large flavour-changing neutral currents, even for a left-right symmetry breaking scale of a few TeV. This originates from the structure of the couplings of the $SU(2)_{R'}$ charged gauge boson W_R, which always interacts with a pair of fermions comprising one SM fermion and one exotic, heavier, fermion. Consequently, the W_R boson can neither be be produced from, nor decay into, a pair of ordinary quarks (or leptons), and its mass is thus free from any constraints that could be imposed from direct searches for extra gauge bosons at the LHC. Moreover, this boson does not mix with the charged SM W ($\equiv W_L$) gauge boson. Consequently, the W_R boson can be much lighter than in conventional LRSM scenarios. However indirect bounds on the W_R mass exists through the relation between its mass and that of the additional neutral gauge boson Z', which can be produced and decay in the ordinary way and that is also allowed to mix with the neutral SM Z boson. The most stringent bounds on the mass of the ALRM W_R boson consequently arise indirectly from the bounds that are imposed on the mass of the neutral Z' boson [16, 17], through the relation between the masses of the two new bosons [14].

Furthermore, previous studies have established conditions for the stability of the ALRM vacuum state [18], demonstrated the model's potential impact on neutrinoless double beta decay processes and leptogenesis [19], and shown that exotic fermions and Higgs bosons could indirectly influence rare top decays [20]. Notably, ALRM setup offers the possibility of significant enhancements in the corresponding branching ratios relative to the SM predictions, with predicted values close to the current limits. Building upon these last findings, we explore the implications of ALRM for rare lepton-flavour-violating (LFV) processes and on the anomalous magnetic moment of the muon a_μ, and we investigate the extent to which this could yield potential constraints on the masses in the model. Loop effects are expected to be sensitive to contributions involving W_R-boson exchanges, so bounds on the considered processes could lead to W_R mass limits stronger than the indirect collider bounds derived from Z' constraints. This would highlight an interesting complementarity between direct searches for extra gauge bosons at colliders and indirect bounds from rare LFV processes and a_μ. While collider mass limit on ALRM Z' bosons lead to indirect bounds on the W_R state, the non-observation of rare LFV processes and the expected size of the new physics contributions to a_μ would constrain not only the W_R boson itself, but also the Z' state indirectly, via the corresponding mass relations.

The structure of the paper is as follows. In Section II, we briefly review the field content of the ALRM, the associated Lagrangian and relevant relations between the physical masses and the free parameters in the model. Section III is dedicated to a study of the impact of the one-loop and two-loop ALRM contributions to the anomalous magnetic moment of the muon and the extraction of associated constraints, while in Section IV we focus on rare LFV processes such as $\mu \to e\gamma$ and $\mu - e$ conversions in various nuclei, and compare predictions to present and future bounds. We present our conclusions in Section V.

II. DESCRIPTION OF THE ALRM FRAMEWORK

The ALRM relies on the $\mathcal{G}_{\mathrm{ALRM}} = SU(3)_C \otimes SU(2)_L \otimes SU(2)_{R'} \otimes U(1)_{B-L}$ gauge symmetry, supplemented by an additional $U(1)_S$ global symmetry. The generator of this global symmetry, along with the third generator of $SU(2)_{R'}$,

allows for the definition of a conserved generalised lepton number and dark matter stability. The spontaneous breaking of $SU(2)_{R'} \otimes U(1)_{B-L} \otimes U(1)_S$ to the hypercharge group is implemented by means of an $SU(2)_{R'}$ doublet of Higgs fields χ_R charged under $U(1)_{B-L}$, while the breaking of $SU(2)_L \otimes U(1)_Y$ to electromagnetism proceeds via a bi-doublet of Higgs fields charged under both $SU(2)_L$ and $SU(2)_{R'}$, with zero $B-L$ charge. Furthermore, to maintain left-right symmetry, the scalar sector of the model includes an $SU(2)_L$ doublet χ_L. The complete field content of the ALRM scalar sector, along with the quantum numbers under $\mathcal{G}_{ALRM} \otimes U(1)_S$, is provided in the left panel of Table I. The structure of the vacuum corresponding to the breaking pattern mentioned above is given by

$$\langle \Phi \rangle = \frac{1}{\sqrt{2}} \begin{pmatrix} 0 & 0 \\ 0 & k \end{pmatrix}, \qquad \langle \chi_L \rangle = \frac{1}{\sqrt{2}} \begin{pmatrix} 0 \\ v_L \end{pmatrix}, \qquad \langle \chi_R \rangle = \frac{1}{\sqrt{2}} \begin{pmatrix} 0 \\ v_R \end{pmatrix}, \tag{1}$$

where the component field ϕ_1^0 is protected from acquiring a vacuum expectation value (VEV) by the conservation of the generalised lepton number.

The central and right panels of Table I present the fermionic field content of the model. It includes the conventional $SU(2)_L$ doublets of left-handed quarks and leptons, Q_L and L_L, as well as the $SU(2)_L$ singlets of right-handed down-type quarks d_R and neutrinos ν_R. All these fields are also $SU(2)_{R'}$ singlets. Additionally, the model features two $SU(2)_{R'}$ doublets that pair the SM right-handed quark u_R and charged lepton e_R with two exotic fermions, a right-handed down-type quark d'_R and a scotino n_R, respectively. Moreover, to preserve the left-right symmetry, the model also contains two exotic $SU(2)_{R'}$ singlets, a new left-handed down-type quark d'_L and a left-handed scotino n_L. All fermionic fields become massive after the breaking of $\mathcal{G}_{ALRM}$ to electromagnetism, and those with the same quantum numbers mix. However, the conservation of the generalised lepton number forbids scotino/neutrino and SM/exotic down-type quark mixings, and also prevents the $SU(2)_L$ and $SU(2)_{R'}$ charged gauge bosons $W \equiv W_L$ and W_R from mixing.

The model Lagrangian includes standard gauge-invariant kinetic terms for all fields, as well as Yukawa interactions between the Higgs sector and the fermions,

$$\mathcal{L}_Y = -\bar{Q}_L Y^q \tilde{\Phi}^\dagger Q_R - \bar{Q}_L Y_L^q \chi_L d_R - \bar{Q}_R Y_R^q \chi_R d'_L - \bar{L}_L Y^\ell \Phi L_R - \bar{L}_L Y_L^\ell \tilde{\chi}_L^\dagger \nu_R - \bar{L}_R Y_R^\ell \tilde{\chi}_R^\dagger n_L + \bar{\nu}_R^c M \nu_R + \text{H.c.} \tag{2}$$

In our notation, the Yukawa couplings Y are 3×3 matrices in the flavour space (with generation indices not shown for clarity). The soft $U(1)_S$ symmetry breaking term, $\bar{\nu}_R^c M \nu_R$ (with M being also a 3×3 matrix in the flavour space), is introduced to generate neutrino masses via seesaw mechanism. This implies relations between the neutrino and scotino mass eigenstates ν, N, $\hat{n}$ and their flavour-eigenstate counterparts via five 3×3 mixing matrices $\mathcal{V}^{\nu\nu}$, $\mathcal{V}^{\nu N}$, $\mathcal{V}^{N\nu}$, $\mathcal{V}^{NN}$ and $\mathcal{V}^{nn}$,

$$\nu_{\alpha L} = \mathcal{V}_{\alpha i}^{\nu\nu} \nu_i + \mathcal{V}_{\alpha j}^{\nu N} N_j, \qquad \nu_{Ri} = \mathcal{V}_{ij}^{N\nu} \nu_j + \mathcal{V}_{ij}^{NN} N_j, \qquad n_{Ri} = \mathcal{V}_{ij}^{nn} \hat{n}_{Rj} \tag{3}$$

where $\alpha = e, \mu, \tau$ and $(i,j) = 1,2,3$. Furthermore, we have absorbed all scotino rotations into a redefinition of the right-handed scotino basis $\{n_R\} \to \{\hat{n}_R\}$, the $\{n_L\} = \{\hat{n}_L\}$ field basis being unchanged.

The multiscalar interactions are encoded in the scalar potential

$$V = \kappa \big[\chi_L^\dagger \Phi \chi_R + \chi_R^\dagger \Phi^\dagger \chi_L \big] - \mu_1^2 \text{Tr} \big[\Phi^\dagger \Phi \big] - \mu_2^2 \big[\chi_L^\dagger \chi_L + \chi_R^\dagger \chi_R \big] + \lambda_1 \big(\text{Tr} \big[\Phi^\dagger \Phi \big] \big)^2 + \lambda_2 \, (\Phi \cdot \tilde{\Phi})(\tilde{\Phi}^\dagger \cdot \Phi^\dagger)$$
$$+ \lambda_3 \Big[\big(\chi_L^\dagger \chi_L \big)^2 + \big(\chi_R^\dagger \chi_R \big)^2 \Big] + 2\lambda_4 \, \big(\chi_L^\dagger \chi_L \big) \, \big(\chi_R^\dagger \chi_R \big) + 2\alpha_1 \text{Tr} \big[\Phi^\dagger \Phi \big] \big[\chi_L^\dagger \chi_L + \chi_R^\dagger \chi_R \big] \tag{4}$$
$$+ 2\alpha_2 \big[\big(\chi_L^\dagger \Phi \big) \big(\chi_L \Phi^\dagger \big) + \big(\Phi^\dagger \chi_R^\dagger \big) \, \big(\Phi \chi_R \big) \big] + 2\alpha_3 \big[\big(\chi_L^\dagger \tilde{\Phi}^\dagger \big) \, \big(\chi_L \tilde{\Phi} \big) + \big(\tilde{\Phi} \chi_R^\dagger \big) \, \big(\tilde{\Phi}^\dagger \chi_R \big) \big],$$

that includes bilinear (μ), trilinear (κ) and quartic (λ, α) terms. After the breaking of the $\mathcal{G}_{ALRM} \otimes U(1)_S$ symmetry, all scalar fields with the same electric charge mix, with the exception of ϕ_1^0 which is protected from mixing by the conservation of the generalised lepton number. The physical states thus contain four CP-even Higgs bosons H_1^0, H_2^0, H_3^0 and the SM Higgs h, two CP-odd Higgs bosons A_1^0 and A_2^0, and two pairs of charged Higgs bosons $H_1^\pm$, $H_2^\pm$. Additionally the set of mixed eigenstates includes two neutral and two charged massless Goldstone bosons G_1^0, G_2^0, $G_1^\pm$ and $G_2^\pm$, which are absorbed by the neutral and charged gauge bosons as their longitudinal degrees of freedom. All these states are related to the various gauge eigenstates of Table I via unitary rotations,

$$\Im\{\phi_1^0\} = A_1^0, \quad \Re\{\phi_1^0\} = H_1^0, \quad \begin{pmatrix} \Im\{\phi_2^0\} \\ \Im\{\chi_L^0\} \\ \Im\{\chi_R^0\} \end{pmatrix} = U_{3\times3}^{\text{A}} \begin{pmatrix} A_2^0 \\ G_1^0 \\ G_2^0 \end{pmatrix}, \quad \begin{pmatrix} \Re\{\phi_2^0\} \\ \Re\{\chi_L^0\} \\ \Re\{\chi_R^0\} \end{pmatrix} = U_{3\times3}^{\text{H}} \begin{pmatrix} h \\ H_2^0 \\ H_3^0 \end{pmatrix},$$
$$\begin{pmatrix} \phi_2^\pm \\ \chi_L^\pm \end{pmatrix} = \begin{pmatrix} \cos\beta & \sin\beta \\ -\sin\beta & \cos\beta \end{pmatrix} \begin{pmatrix} H_1^\pm \\ G_1^\pm \end{pmatrix}, \qquad \begin{pmatrix} \phi_1^\pm \\ \chi_R^\pm \end{pmatrix} = \begin{pmatrix} \cos\zeta & \sin\zeta \\ -\sin\zeta & \cos\zeta \end{pmatrix} \begin{pmatrix} H_2^\pm \\ G_2^\pm \end{pmatrix}. \tag{5}$$

Analytical expressions for the two 3×3 mixing matrices $U_{3\times3}^{\mathrm{A}}$ and $U_{3\times3}^{\mathrm{H}}$ in terms of the model's free parameters can be found in [14], while the two mixing angles β and ζ are defined by

$$\tan\beta = k/v_L, \quad \text{and} \quad \tan\zeta = k/v_R. \tag{6}$$

The breaking of the left-right symmetry also generates masses for the model gauge bosons, and induces their mixing. The charged $W \equiv W_L$ and $W' \equiv W_R$ bosons do not mix, as $\langle \phi_1^0 \rangle = 0$, and their masses are given by

$$M_{W_L} = \frac{1}{2} g_L \sqrt{k^2 + v_L^2} \equiv \frac{1}{2} g_L v \quad \text{and} \quad M_{W_R} = \frac{1}{2} g_R \sqrt{k^2 + v_R^2} \equiv \frac{1}{2} g_R v', \tag{7}$$

with g_L and g_R standing for the $SU(2)_L$ and $SU(2)_{R'}$ gauge coupling constants. In contrast, in the neutral sector, all states mix. The corresponding gauge boson squared mass matrix reads, in the $(B_\mu, W_{L\mu}^3, W_{R\mu}^3)$ basis,

$$(\mathcal{M}_V^0)^2 = \frac{1}{4} \begin{pmatrix} g_{B-L}^2 \, (v_L^2 + v_R^2) & -g_{B-L} \, g_L \, v_L^2 & -g_{B-L} \, g_R \, v_R^2 \\ -g_{B-L} \, g_L \, v_L^2 & g_L^2 \, v^2 & -g_L \, g_R \, k^2 \\ -g_{B-L} \, g_R \, v_R^2 & -g_L \, g_R \, k^2 & g_R^2 \, v'^2 \end{pmatrix}, \tag{8}$$

where g_{B-L} refers to the $B-L$ gauge coupling constant. This matrix can be diagonalised through three independent rotations that mix the B, W_L^3 and W_R^3 bosons into the massless photon A and massive Z and Z' states,

$$\begin{pmatrix} B_\mu \\ W_{L\mu}^3 \\ W_{R\mu}^3 \end{pmatrix} = \begin{pmatrix} \cos\phi_W & 0 & -\sin\phi_W \\ 0 & 1 & 0 \\ \sin\phi_W & 0 & \cos\phi_W \end{pmatrix} \begin{pmatrix} \cos\theta_W & -\sin\theta_W & 0 \\ \sin\theta_W & \cos\theta_W & 0 \\ 0 & 0 & 1 \end{pmatrix} \begin{pmatrix} 1 & 0 & 0 \\ 0 & \cos\zeta_W & -\sin\zeta_W \\ 0 & \sin\zeta_W & \cos\zeta_W \end{pmatrix} \begin{pmatrix} A_\mu \\ Z_\mu \\ Z'_\mu \end{pmatrix}. \tag{9}$$

The ϕ_W-rotation mixes the B and W_R^3 bosons into the hypercharge boson B', the θ_W-rotation corresponds to the usual electroweak mixing, and the ζ_W-rotation is related to the strongly constrained Z/Z' mixing. The various mixing angles are related to the different gauge coupling constants and VEVs,

$$\sin\phi_W = \frac{g_{B-L}}{\sqrt{g_{B-L}^2 + g_R^2}} = \frac{g_Y}{g_R} \quad \text{and} \quad \sin\theta_W = \frac{g_Y}{\sqrt{g_L^2 + g_Y^2}} = \frac{e}{g_L},$$

$$\tan(2\zeta_W) = \frac{2\cos\phi_W \cos\theta_W g_L g_R(\cos^2\phi_W k^2 - \sin^2\phi_W v_L^2)}{-(g_L^2 - \cos^2\phi_W \cos^2\theta_W g_R^2)\cos^2\phi_W k^2 - (g_L^2 - \cos^2\theta_W g_{B-L}^2 \sin^2\phi_W)\cos^2\phi_W v_L^2 + \cos_W^\theta 2 g_R^2 v_R^2}. \tag{10}$$

where in these expressions, g_Y and e denote the usual hypercharge and electromagnetic coupling constant respectively. Neglecting the Z/Z' mixing (i.e., when $\zeta_W \to 0$), the Z and Z' boson masses are given through the compact expressions

$$M_Z = \frac{g_L}{2\cos\theta_W} v \quad \text{and} \quad M_{Z'} = \frac{1}{2}\sqrt{g_{B-L}^2 \sin^2\phi_W v_L^2 + \frac{g_R^2(\cos^4\phi_W k^2 + v_R^2)}{\cos^2\phi_W}}. \tag{11}$$

With a particle spectrum including multiple new charged and neutral scalars and gauge bosons interacting directly with the leptons, the ALRM model can potentially influence many lepton-flavour-violating processes, and impact significantly predictions for the anomalous magnetic dipole moments of the charged leptons. The main purpose of this work is to explore this possibility, and identify regions of the parameter space that are phenomenologically interesting.

III. THE ANOMALOUS MAGNETIC MOMENT OF THE MUON

Despite the fact that the gyromagnetic ratio of muon (g_μ) is precisely 2 at tree level, significant quantum corrections arise from loop contributions. Measurements of the anomalous magnetic moment of the muon, denoted by $a_\mu = \frac{g_\mu - 2}{2}$, could thus provide an excellent probe of physics Beyond the Standard Model (BSM). In the SM, the predicted value for a_μ, with its uncertainty, has been evaluated by the Muon $g - 2$ Theory Initiative in 2020 as [21–38]:

$$a_\mu^{\mathrm{SM}} = (116591810 \pm 43) \times 10^{-11}. \tag{12}$$

This value relies on the most up-to-date QED predictions, that are supplemented with electroweak, hadronic vacuum polarisation, and hadronic light-by-light contributions. On the other hand, the latest findings from the E989 experiment at Fermilab [39] provide the most precise measurement of the anomalous magnetic moment to date, $a_\mu^{\mathrm{expt\cdot}}(\mathrm{FNAL}) = (116592040 \pm 54) \times 10^{-11}$ [40], while the previous result from the Brookhaven National Laboratory
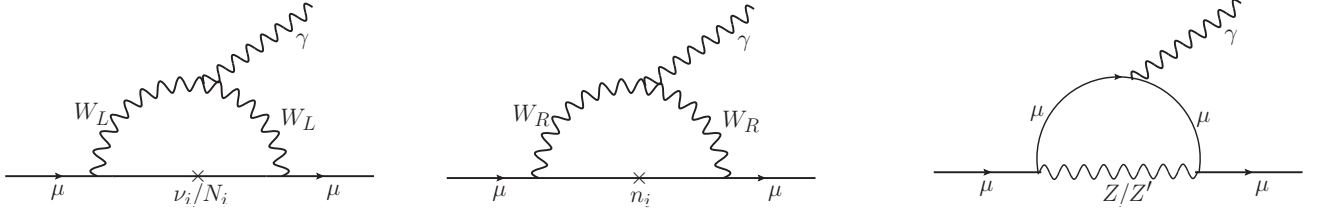
FIG. 1: Representative Feynman diagrams contributing to a_μ and involving gauge couplings of the model's fermions.
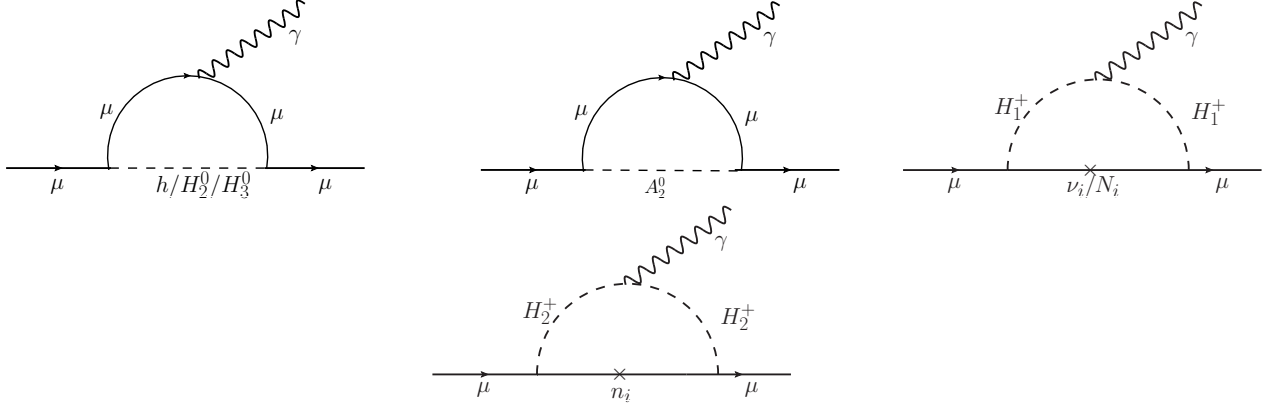

FIG. 2: Representative Feynman diagrams contributing to a_μ and involving the model's scalars.

is $a_\mu^{\text{expt.}}(\text{BNL}) = (116592089 \pm 63) \times 10^{-11}$. The combination of these two measurements has yielded a new world average experimental value,

$$a_\mu^{\text{expt.}}(\text{Comb}) = (116592061 \pm 41) \times 10^{-11} \,, \tag{13}$$

which confirms and sharpens the discrepancy Δa_μ between experimental observations and the SM prediction (12) to a level of 4.2σ. The quantity Δa_μ, estimated in [41] as

$$\Delta a_\mu = a_\mu^{\text{expt.}}(\text{Comb}) - a_\mu^{\text{SM}} = (251 \pm 59) \times 10^{-11} \,, \tag{14}$$

can thus be used as a good motivation for various BSM scenarios. However, recent lattice simulations of the hadronic vacuum polarisation contribution to a_μ have suggested a reconciliation between theoretical predictions and experimental measurements [42–46], while also revealing discrepancies in the properties of $e^+e^- \to \pi^+\pi^-$ scattering [47]. As a result, while the likelihood of large new physics contributions to a_μ has diminished, unresolved issues remain and continue to motivate BSM explorations in this context. This leaves open the question of whether the deviation (14) should still be interpreted as a sign of new physics affecting hadronic vacuum polarisation. If this interpretation holds, one must keep in mind that such contributions generally worsen electroweak precision fits. Conversely, models predicting smaller contributions to a_μ may become increasingly attractive in light of the recent lattice findings (and a negative answer to the above question). One-loop electroweak corrections to the muon anomalous magnetic moment were first computed over five decades ago [48–54], and comprehensive reviews discussing the computation of both SM and BSM contributions can be found in [38, 55, 56]. Additionally, several studies have explored new physics contributions to the anomalous magnetic moment at the one-loop level within specific theoretical frameworks [57–60].

As the ALRM introduces additional (exotic) fermions, scalars and gauge bosons, it is important to assess their impact on predictions for a_μ, together with the associated consequences on the parameter space of the model. In this work, we analyze one-loop and two-loop (Barr-Zee) contributions in turn.

A. One-loop contributions

In our model, one-loop contributions involving massive gauge and scalar bosons to Δa_μ arise from the Feynman diagrams given in Figs. 1 and 2, that represent contributions proportional to the model's gauge couplings and those involving the couplings of the model's scalars, respectively. The first set of contributions involving gauge bosons

yields [38, 55, 56]:

$$\Delta a_\mu(W_L) = \frac{1}{4\pi^2} \left(\frac{m_\mu^2}{M_{W_L}^2}\right) \frac{5}{6} \frac{g_L^2}{4} \left[|\mathcal{V}_{\mu i}^{\nu\nu}|^2 + |\mathcal{V}_{\mu i}^{\nu N}|^2\right],$$

$$\Delta a_\mu(W_R) = \frac{1}{4\pi^2} \left(\frac{m_\mu^2}{M_{W_R}^2}\right) \frac{5}{6} \frac{g_R^2}{4} |\mathcal{V}_{\mu i}^{nn}|^2,$$

$$\Delta a_\mu(Z) = -\frac{1}{4\pi^2} \left(\frac{m_\mu^2}{M_Z^2}\right) \left(\frac{e^2}{12}\right) \left[\frac{g_L^2}{g_Y^2} - \frac{g_Y^2}{g_L^2} + 4\right],$$

$$\Delta a_\mu(Z') = -\frac{1}{4\pi^2} \left(\frac{m_\mu^2}{M_{Z'}^2}\right) \left(\frac{e^2}{12}\right) \left(\frac{g_R^2}{g_Y^2} - \frac{g_Y^2}{g_R^2} - 1\right) / \left(\frac{1}{g_Y^2} - \frac{1}{g_R^2}\right), \tag{15}$$

while the second set of diagrams involving scalars gives [55, 56, 61–65]:

$$\Delta a_\mu(h) = \frac{1}{4\pi^2} \left(\frac{m_\mu^2}{M_h^2}\right) \frac{|Y^\mu|^2}{2} |U_{11}^H|^2 \left[-\frac{7}{12} - \log\left(\frac{m_\mu}{M_h}\right)\right],$$

$$\Delta a_\mu(H_2^0) = \frac{1}{4\pi^2} \left(\frac{m_\mu^2}{M_{H_2^0}^2}\right) \frac{|Y^\mu|^2}{2} |U_{12}^H|^2 \left[-\frac{7}{12} - \log\left(\frac{m_\mu}{M_{H_2^0}}\right)\right],$$

$$\Delta a_\mu(H_3^0) = \frac{1}{4\pi^2} \left(\frac{m_\mu^2}{M_{H_3^0}^2}\right) \frac{|Y^\mu|^2}{2} |U_{13}^H|^2 \left[-\frac{7}{12} - \log\left(\frac{m_\mu}{M_{H_3^0}}\right)\right],$$

$$\Delta a_\mu(A_2^0) = \frac{1}{4\pi^2} \left(\frac{m_\mu^2}{M_{A_2^0}^2}\right) \frac{|Y^\mu|^2}{2} |U_{11}^A|^2 \left[\frac{11}{12} + \log\left(\frac{m_\mu}{M_{A_2^0}}\right)\right],$$

$$\Delta a_\mu(H_1^+) = -\frac{1}{4\pi^2} \left(\frac{m_\mu^2}{M_{H_1^+}^2}\right) \left(\frac{1}{48}\right) \left(\frac{1}{k^2+v_L^2}\right) \left[|Y^\mu|^2 v_L^2 \left(|\mathcal{V}_{\mu i}^{\nu\nu}|^2 + |\mathcal{V}_{\mu i}^{\nu N}|^2\right) + |Y_L^\mu|^2 k^2 \left(|\mathcal{V}_{\mu i}^{N\nu}|^2 + |\mathcal{V}_{\mu i}^{NN}|^2\right)\right],$$

$$\Delta a_\mu(H_2^+) = -\frac{1}{4\pi^2} \left(\frac{m_\mu^2}{M_{H_2^+}^2}\right) \left(\frac{1}{48}\right) \left(\frac{1}{k^2+v_R^2}\right) |\mathcal{V}_{\mu i}^{nn}|^2 \left[|Y^\mu|^2 v_R^2 + |Y_R^\mu|^2 k^2\right]. \tag{16}$$

The interaction vertices and the corresponding couplings are listed in the tables given in Appendix A, where, as in the rest of this work, we conveniently denote all scotino mass eigenstates by $n \equiv \hat{n}$ to simplify the notation. In order to assess the impact of these diagrams quantitatively, we implement a random scan of the model's parameter space in which we allow the free parameters of the model to vary in the following ranges:

$$\begin{aligned}
\text{gauge couplings}: \quad & g_L = 0.65, \quad g_R \in [0.37, 1], \\
\text{VEVs}: \quad & k = 246 \text{ GeV}, \quad v_R \in [6.5, 50] \text{ TeV}, \quad \tan\beta \in [25, 50], \\
\text{Trilinear couplings}: \quad & \kappa \in [-3000, -10] \text{ GeV}, \\
\text{Exotic lepton masses}: \quad & m_{n_1, n_2, n_3} \in [1, 10^5] \text{ GeV}, \\
\text{Neutrino sector masses}: \quad & M_{N_1} = 10^3 \text{ GeV}, M_{N_2} = 10^{3.5} \text{ GeV}, M_{N_3} = 10^4 \text{ GeV}, \\
& m_\nu^{\text{lightest}} \in [10^{-6}, 0.01] \text{ eV}, \\
\text{Other Yukawa couplings}: \quad & Y^\mu = \frac{\sqrt{2} m_\mu}{k} = 6.08 \times 10^{-4}, Y^e = \frac{\sqrt{2} m_e}{k} = 2.94 \times 10^{-6}, \tag{17}
\end{aligned}$$

where $Y^e \equiv (Y^\ell)_{11}$ and $Y^\mu \equiv (Y^\ell)_{22}$. Furthermore, the active neutrino oscillation parameters are taken such that they lie within 3σ of their experimental value [66],

$$\Delta m_{21}^2 \in [6.81, 8.03] \times 10^{-5} \text{eV}^2, \quad |\Delta m_{31}^2| \in [2.428, 2.597] \times 10^{-3} \text{eV}^2, \quad \delta_{\text{CP}} \in [108°, 404°],$$

$$\sin^2\theta_{12} \in [0.275, 0.344], \quad \sin^2\theta_{23} \in [0.407, 0.620], \quad \sin^2\theta_{13} \in [0.02029, 0.02319], \tag{18}$$

while the heavy neutrino and scotino mixing angles are varied over the range $[0, \pi/2]$ with a zero CP-violating Dirac phase. Considering a normal hierarchical active neutrino mass ordering, the masses of the second and third neutrinos are given by

$$m_{\nu_2} = \sqrt{(m_\nu^{\text{lightest}})^2 + \Delta m_{21}^2}, \quad m_{\nu_3} = \sqrt{(m_\nu^{\text{lightest}})^2 + |\Delta m_{31}^2|},$$

while the general 3×3 active neutrino mass matrix m_ν can be determined from

$$m_\nu = \mathcal{V}^{\nu\nu} m_\nu^{\text{diag}} (\mathcal{V}^{\nu\nu})^T \quad \text{with} \quad m_\nu^{\text{diag}} = \text{diag}\left[m_\nu^{\text{lightest}}, m_{\nu_2}, m_{\nu_3}\right]. \tag{19}$$
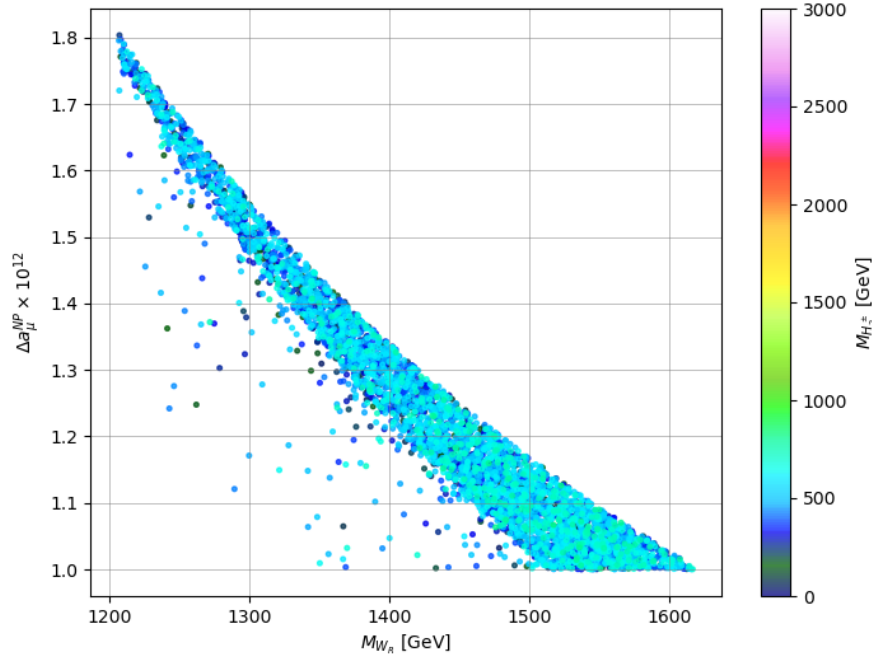
FIG. 3: New physics one-loop contribution $\Delta a_\mu^{\mathrm{NP}}$ to the anomalous magnetic moment of the muon in the ALRM. Each point represents one benchmark explored in our random parameter space scan, and predictions for $\Delta a_\mu^{\mathrm{NP}}$ are displayed as a function of the mass of the $SU(2)_R$ boson, M_{W_R}. In addition, the colour code refers to the mass of the second charged Higgs boson, $M_{H_2^\pm}$, and we have only considered scenarios in which the Z' mass satisfies $M_{Z'} > 4.5$ TeV. For clarity, scenarios for which $\Delta a_\mu^{\mathrm{NP}} < 10^{-12}$ have been omitted.

The remaining Yukawa couplings, that we consider diagonal, are fully determined once all the parameters above are fixed,

$$(Y_L^\ell)^{\mathrm{diag}} = \frac{\sqrt{2 m_\nu^{\mathrm{diag}} M_N^{\mathrm{diag}}}}{v_L} \qquad \text{with} \qquad M_N^{\mathrm{diag}} = \mathrm{diag}\,[\mathrm{M}_{\mathrm{N}_1}, \mathrm{M}_{\mathrm{N}_2}, \mathrm{M}_{\mathrm{N}_3}],$$

$$(Y_R^\ell)^{\mathrm{diag}} = (\mathcal{V}^{nn})^\dagger Y_R^\ell \mathcal{V}^{nn} = \frac{\sqrt{2} m_n^{\mathrm{diag}}}{v_R} \qquad \text{with} \qquad m_n^{\mathrm{diag}} = \mathrm{diag}\,[\mathrm{m}_{\mathrm{n}_1}, \mathrm{m}_{\mathrm{n}_2}, \mathrm{m}_{\mathrm{n}_3}].$$

(20)

Correspondingly, the general 3×3 scotino mass matrix can be rewritten as $m_n = \mathcal{V}^{nn} m_n^{\mathrm{diag}} (\mathcal{V}^{nn})^\dagger$. Here scotinos are Dirac fermions such that, without loss of generality, we have assumed that the same unitary mixing matrices could be used to diagonalise its left-handed and right-handed sectors for simplicity.

In Fig. 3, we present the total contribution of Δa_μ from all diagrams mentioned above against W_R-mass, M_{W_R} and after imposing existing LHC bounds on M_{W_R} via existing Z' mass limits (through the associated tree-level mass relations). Consequently, M_{W_R} has to be larger than approximately 1200 GeV [14]. In addition, our colour scheme indicates the value of the mass of the second charged Higgs state for each point in the scan. It is found to span a large range of values, although our results show in particular that the lightest charged Higgs $H_2^\pm$ can be light with mass of a few hundreds GeV. On the other hand, all other non-SM neutral Higgs bosons H_1^0, H_2^0 and H_3^0 are found much heavier throughout the whole parameter scan, with masses greater than 5 TeV, and for most of the points the heaviest charged Higgs boson has a mass lying below 1 TeV [14, 18]. We opted to focus on the two bosons W_R and $H_2^\pm$ as they are the most relevant ones in light of the analytical results presented in Eqs. (15) and (16) and the chosen set of input parameters. Notice that the other charged Higgs, H_1^+ is much heavier than H_2^+. Our predictions show that ALRM one-loop contributions to a_μ increase with decreasing M_{W_R} mass values. This different behaviour is inherent to the dependence of the scalar contributions on the various Higgs VEVs, that is absent for diagrams with only gauge-boson exchanges. Nevertheless, for the scanned values of M_{W_R} and v_R consistent with the constraints imposed and for the whole range of variations in the input parameters, the new physics contributions to the anomalous magnetic moment of the muon are still three orders of magnitude smaller than what would be required to get consistency between the

FIG. 4: Representative new physics Feynman diagrams contributing to the anomalous magnetic moment of the muon at two loop in the ALRM.

experiment and the prediction of the Muon $g-2$ Theory initiative given in Eq. (15). On the other hand, accounting for the newest lattice results would not challenge the viability of the model, despite a rich leptonic sector.

While these findings are encouraging, we now proceed to investigate ALRM two-loop contributions to a^μ, as the latter could be significant for new physics setups allowing for new heavy fermions to circulate in the loops.

B.   Two-loop contributions

The different class of (Barr-Zee) [67, 68] Feynman diagrams responsible for two-loop ALRM contributions to the muon anomalous magnetic moment are shown in Fig. 4. Analytical expressions for the first three class of diagrams,

$\Delta a_\mu^{(i)}$ with $i = 1, 2, 3$, are given by [62, 63, 65, 69–71, 71, 72]

$$\Delta a_\mu^{(1)} = \frac{e^2 m_\mu^2}{128\pi^4 v^2} \sum_{\phi_i^0, f_1} N_C^f \, Q_f^2 \, Y_f^{\phi_i^0} Y_\mu^{\phi_i^0} \, G_{\phi_i^0}^{(1)} \left(\frac{m_{f_1}^2}{M_{\phi_i^0}^2} \right),$$

$$\Delta a_\mu^{(2)} = \frac{e^2 m_\mu^2}{64\pi^4 M_{\phi_i^0}^2} \sum_{\phi_i^0} Y_\mu^{\phi_i^0} \, \lambda_{\phi_i^0 H_{1,2}^+ H_{1,2}^-} \, G^{(2)} \left(\frac{M_{H_{1,2}^\pm}^2}{M_{\phi_i^0}^2} \right), \qquad (21)$$

$$\Delta a_\mu^{(3)} = \frac{e^2 m_\mu^2}{128\pi^4 v^2} \sum_{\phi_i^0} Y_\mu^{\phi_i^0} Y_W^{\phi_i^0} G^{(3)} \left(\frac{M_{W_{L,R}}^2}{M_{\phi_i^0}^2} \right).$$

Here, the M_i parameters stand for the physical masses of the different bosonic states, the m_i parameters for the masses of the quarks and charged leptons in the model, and the Yukawa couplings $Y_f^{\phi_i^0}$ and $Y_\mu^{\phi_i^0}$ are the strengths of the $\bar{f} f \phi_i^0$ and $\bar{\mu} \mu \phi_i^0$ interactions, respectively, with the generic fermion $f \equiv t, b, \tau, d', s', b'$ and the generic scalar state $\phi_i^0 \equiv h, H_2^0, H_3^0, A_2^0$. Explicit expressions for these couplings can be found in the tables given in Appendix A. In addition, these two-loop contributions depend on the number of colours N_C^f related to a specific fermion f, the related electric charge Q_f and the three kinds of G functions defined by

$$G_{h/H_2^0/H_3^0}^{(1)}(r) = r \int_0^1 dx \frac{2x(1-x)-1}{x(1-x)-r} \ln \left[\frac{x(1-x)}{r} \right],$$

$$G_{A_2^0}^{(1)}(r) = r \int_0^1 dx \frac{1}{x(1-x)-r} \ln \left[\frac{x(1-x)}{r} \right]$$

$$G^{(2)}(r) = \int_0^1 dx \frac{x(x-1)}{x(1-x)-r} \ln \left[\frac{x(1-x)}{r} \right] \qquad (22)$$

$$G^{(3)}(r) = \frac{1}{2} \int_0^1 dx \frac{x[3x(4x-1)+10]r - x(1-x)}{x(1-x)-r} \ln \left[\frac{x(1-x)}{r} \right].$$

The contributions of the diagram of category $4a$ and $4b$ (first two diagrams of the second line in Fig. 4) read [72]

$$\Delta a_\mu^{(4a)} = \frac{m_\mu^2}{256\pi^4} \frac{1}{\left(M_{H_1^\pm}^2 - M_{W_L}^2 \right)} \sum_{\phi_i^0} (Y_{\mu\nu_i H_1^\pm} g_{\mu\nu_i W_L^\pm} + Y_{\mu N_i H_1^\pm} g_{\mu N_i W_L^\pm}) \lambda_{\phi_i^0 H_1^+ H_1^-} g_{W_L^- H_1^+ \phi_i^0}$$

$$\times \int_0^1 dx \, x^2(x-1) \left[F \left(1, \frac{M_{\phi_i^0}^2}{M_{H_1^\pm}^2} \right) - F \left(\frac{M_{H_1^\pm}^2}{M_{W_L}^2}, \frac{M_{\phi_i^0}^2}{M_{W_L}^2} \right) \right],$$

$$\Delta a_\mu^{(4b)} = \frac{m_\mu^2}{256\pi^4} \frac{1}{\left(M_{H_2^\pm}^2 - M_{W_R}^2 \right)} \sum_{\phi_i^0} Y_{\mu n_i H_2^\pm} \lambda_{\phi_i^0 H_2^+ H_2^-} g_{W_R^- H_2^+ \phi_i^0} g_{\mu n_i W_R^\pm} \qquad (23)$$

$$\times \int_0^1 dx \, x^2(x-1) \left[F \left(1, \frac{M_{\phi_i^0}^2}{M_{H_2^\pm}^2} \right) - F \left(\frac{M_{H_2^\pm}^2}{M_{W_R}^2}, \frac{M_{\phi_i^0}^2}{M_{W_R}^2} \right) \right],$$

and depend on some multiscalar and gauge couplings given explicitly in Appendix A, as well as on the function F defined by

$$F(r_1, r_2) = \int_0^1 dx \frac{\ln \left(\frac{r_1 x + r_2(1-x)}{x(1-x)} \right)}{x(1-x) - r_1 x - r_2(1-x)}. \qquad (24)$$

The same function also appears in the contributions from the last four diagrams, labeled $5a$, $5b$, $6a$ and $6b$, that are given by [72]

$$
\begin{aligned}
\Delta a_\mu^{(5a)} &= \frac{m_\mu^2}{256\pi^4 v^2}\frac{1}{\left(M_{H_1^\pm}^2 - M_{W_L}^2\right)}\sum_{\phi_i^0}(Y_{\mu\nu_i H_1^\pm}g_{\mu\nu_i W_L^\pm} + Y_{\mu N_i H_1^\pm}g_{\mu N_i W_L^\pm})g_{W_L^- H_1^+ \phi_i^0}g_{W_L^+ W_L^- \phi_i^0} \\
&\quad \times \int_0^1 dx\; x^2\left[\left(M_{H_1^\pm}^2 + M_{W_L}^2 - M_{\phi_i^0}^2\right)(1-x) - 4M_{W_L}^2\right]\left[F\left(\frac{M_{W_L}^2}{M_{H_1^\pm}^2}, \frac{M_{\phi_i^0}^2}{M_{H_1^\pm}^2}\right) - F\left(1, \frac{M_{\phi_i^0}^2}{M_{W_L}^2}\right)\right], \\
\Delta a_\mu^{(5b)} &= \frac{m_\mu^2}{256\pi^4 v^2}\frac{1}{\left(M_{H_2^\pm}^2 - M_{W_R}^2\right)}\sum_{\phi_i^0}Y_{\mu n_i H_2^\pm}g_{\mu n_i W_R^\pm}g_{W_R^- H_2^+ \phi_i^0}g_{W_R^+ W_R^- \phi_i^0} \\
&\quad \times \int_0^1 dx\; x^2\left[\left(M_{H_2^\pm}^2 + M_{W_R}^2 - M_{\phi_i^0}^2\right)(1-x) - 4M_{W_R}^2\right]\left[F\left(\frac{M_{W_R}^2}{M_{H_2^\pm}^2}, \frac{M_{\phi_i^0}^2}{M_{H_2^\pm}^2}\right) - F\left(1, \frac{M_{\phi_i^0}^2}{M_{W_R}^2}\right)\right], \\
\Delta a_\mu^{(6a)} &= \frac{m_\mu^2}{256\pi^4 v^2}\frac{N_C}{\left(M_{H_1^\pm}^2 - M_{W_L}^2\right)}\int_0^1 dx(Y_{\mu\nu_i H_1^\pm}g_{\mu\nu_i W_L^\pm} + Y_{\mu N_i H_1^\pm}g_{\mu N_i W_L^\pm})g_{tb W_L^\pm}\; g_{tb H_1^\pm} \\
&\quad \times [Q_t x + Q_b(1-x)]\left[m_b^2 x(1-x) + m_t^2 x(1+x)\right]\left[F\left(\frac{m_t^2}{M_{H_1^\pm}^2}, \frac{m_b^2}{M_{H_1^\pm}^2}\right) - F\left(\frac{m_t^2}{M_{W_L}^2}, \frac{m_b^2}{M_{W_L}^2}\right)\right], \\
\Delta a_\mu^{(6b)} &= \frac{m_\mu^2}{256\pi^4 v^2}\frac{N_C}{\left(M_{H_2^\pm}^2 - M_{W_R}^2\right)}\sum_{q'=d',s',b'}\int_0^1 dx Y_{\mu n_i H_2^\pm}g_{\mu n_i W_R^\pm}g_{tq' W_R^\pm}\; g_{tq' H_2^\pm} \\
&\quad \times [Q_t x + Q_{q'}(1-x)]\left[m_t^2 x(1+x) + m_{q'}^2 x(1-x)\right]\left[F\left(\frac{m_t^2}{M_{H_2^\pm}^2}, \frac{m_{q'}^2}{M_{H_2^\pm}^2}\right) - F\left(\frac{m_t^2}{M_{W_R}^2}, \frac{m_{q'}^2}{M_{W_R}^2}\right)\right].
\end{aligned}
\tag{25}
$$

We now have all the ingredients to evaluate the total contribution to the anomalous magnetic dipole moment of the muon, that simply consists in the sum of the contributions from all one-loop and two-loop individual diagrams listed above,

$$
\Delta a_\mu^{\text{total}} = \Delta a_\mu^{\text{1-loop}} + \Delta a_\mu^{\text{2-loop}}.
\tag{26}
$$

In Fig. 5, we display the two-loop contributions from each subset of diagrams of Fig 4, as a function of v_R while keeping other parameters fixed to the following values:

$$
\begin{aligned}
&\tan\beta = 30\,, \qquad g_R = 0.386\,, \\
&m_{d'} = 100 \text{ GeV}\,, \qquad m_{s'} = 500 \text{ GeV}\,, \qquad m_{b'} = 150 \text{ GeV}\,, \\
&m_{n_1} = 1412 \text{ GeV}\,, \qquad m_{n_2} = 1290 \text{ GeV}\,, \qquad m_{n_3} = 174 \text{ GeV}\,, \qquad \kappa = -87.6 \text{ GeV}\,, \\
&\theta'_{12} = \theta'_{13} = 4.7°\,, \qquad \theta'_{23} = 9.5°\,.
\end{aligned}
\tag{27}
$$

This allows to illustrate, for a given choice of free parameters (other choices lead to similar conclusions), that despite of the presence of several new particles the ALRM does not predict significant contribution to Δa_μ, neither at one loop nor at two loops.

IV. LEPTON FLAVOUR VIOLATING PROCESSES

In this section, we present predictions for several LFV processes within the ALRM framework. We choose processes that are scrutinised by current high-energy physics experiments so that associated measurements could serve as indirect probes of the model's parameter space. We specifically focus on muon radiative decays and $\mu - e$ conversion processes in Sections IV A and IV B, respectively, as these are expected to provide the most stringent constraints. Nonetheless, the calculations presented below can be straightforwardly applied to rare tau decays like $\tau \to \mu\gamma$ or $\tau \to e\gamma$.

In many BSM scenarios that account for neutrino masses, the GIM suppression inherent to the SM contributions to LFV processes is weakened due to the mixing between left-handed and right-handed neutrino states, leading to significantly enhanced rates [78–86]. In our model, this mixing is forbidden, and the usual BSM enhancement from loops of W bosons and extra neutrinos is absent. However, additional fields still contribute such that potential enhancement may arise from loops involving charged Higgs bosons $H_{1,2}^\pm$ and various neutrino states (ν, N and n). Therefore, it is valuable to compare the ALRM predictions with current experimental limits and future sensitivities, which we summarize in Table II, to get indirect insights on which ALRM scenarios could be phenomenologically viable.
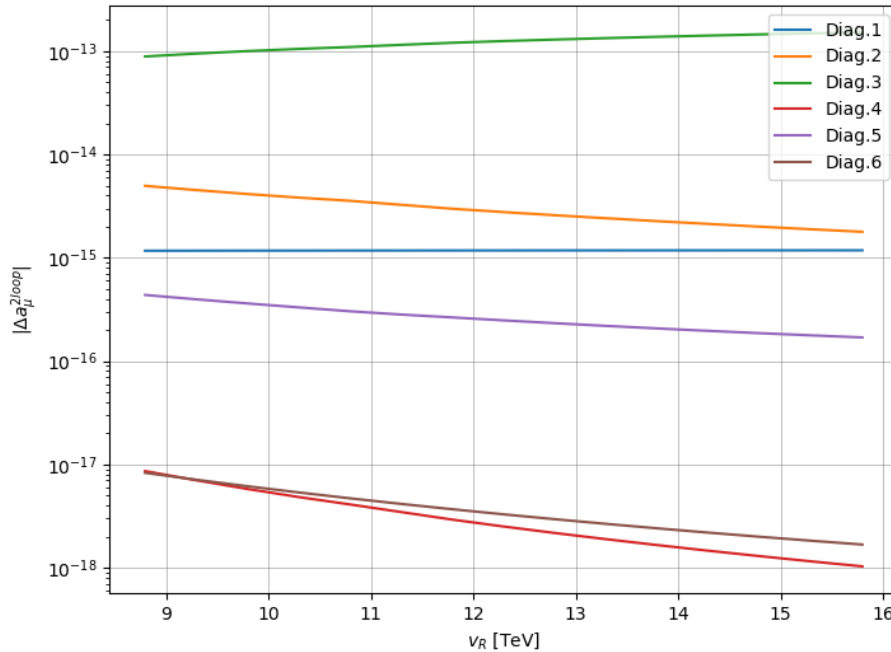
FIG. 5: Two-loop contributions to the anomalous magnetic moment of the muon as a function of v_R, after separating the impact of the different set of diagrams shown in Fig. 4 and for the benchmark scenario defined in Eq. (27).

Process	Present bound	Future sensitivity
BR $(\mu \to e\gamma)$	3.1×10^{-13} [73]	6×10^{-14} [74]
CR $(\mu\text{Au} \to e\text{Au})$	7×10^{-13} [75]	-
CR $(\mu\text{Ti} \to e\text{Ti})$	4.3×10^{-12} [76]	-
CR $(\mu\text{Al} \to e\text{Al})$	-	$10^{-15} - 10^{-17}$ [77]

TABLE II: Current experimental bounds at 90% confidence level on the branching ratio (BR) associated with the muon decay $\mu \to e\gamma$ and on the $\mu - e$ conversion rates (CR) in several nuclei, shown together with expected future sensitivities.

A. Flavour-violating muon decay $\mu \to e\gamma$

Within the SM, $\mu \to e\gamma$ decays are forbidden due to the absence of flavour-changing-neutral currents and the conservation of the lepton flavor. However, in simple BSM extensions featuring neutrino masses and mixings, this process can occur via higher-order loop diagram contributions. In this case, one-loop effects mediated by diagrams comprising neutrinos and W bosons increase the decay rate, although its value is still negligibly small,

$$\text{BR}(\mu \to e\gamma)^{\text{SM}+\nu} \leq 10^{-54}\,. \tag{28}$$

This is consequently far beyond the reach of any current [73] or future experiment (like MEG II [74]), as shown in Table II, which makes this process essentially undetectable in near future.

The amplitude relevant for the $\mu \to e\gamma$ process can be formally written as

$$\mathcal{A}(\mu \to e\gamma) = i\epsilon_\nu^*(q)\,\overline{u}_e(p')\,\sigma^{\nu\mu}q_\mu\left[\mathcal{A}_R P_R + \mathcal{A}_L P_L\right]u_\mu(p)\,, \tag{29}$$

where p, p' and q are the four-momenta of the muon, electron and photon, respectively. Moreover, following standard notation, $P_{L,R} = \frac{1}{2}\left(1 \mp \gamma^5\right)$ represent the left-handed and right-handed chirality projectors, $\sigma^{\mu\nu} = \frac{i}{2}[\gamma^\mu, \gamma^\nu]$, while $\overline{u}_e$, u_μ stand for the electron and muon spinors and ϵ_ν^* for the photon polarisation vector. Squaring and averaging this amplitude allows for the computation of the associated partial decay width, which reads, in terms of the loop
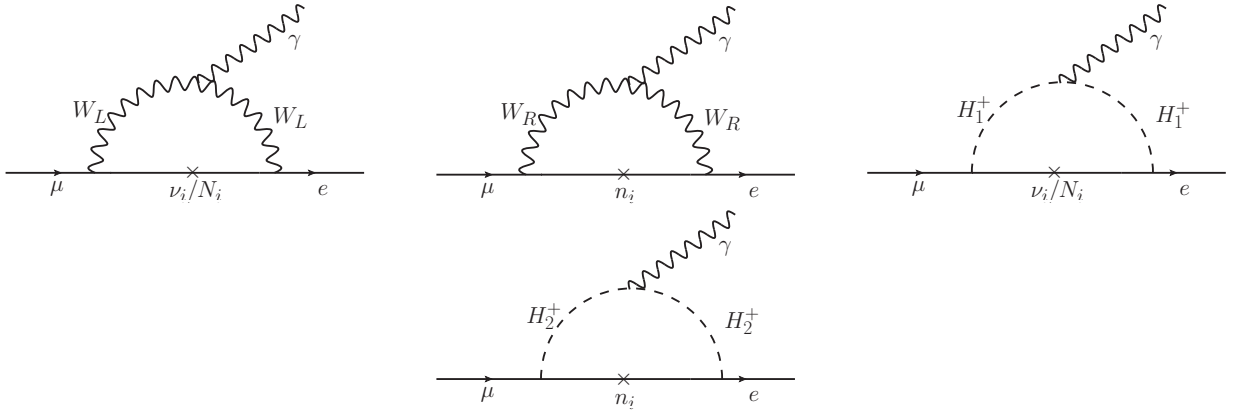
FIG. 6: The Feynman diagrams responsible for $\mu \to e\gamma$ in the ALRM model.

factors $\mathcal{A}_L$ and $\mathcal{A}_R$,

$$\Gamma(\mu \to e\gamma) = \frac{m_\mu^3}{16\pi}\left(|\mathcal{A}_L|^2 + |\mathcal{A}_R|^2\right). \tag{30}$$

In this expression, the electron mass m_e has been neglected while m_μ is the muon mass. In the class of models considered in this work, the presence of a Majorana mass term for the right-handed neutrino state ν_R leads to additional diagrams mediating the muon decay into an electron-photon final state, via loops comprising neutrinos and W bosons. These diagrams, represented by the first diagram in Fig. 6, are similar to those emerging in the SM+ν case. The associated contribution is therefore expected to be negligible and no different from Eq. (28), *i.e* of $\mathcal{O}(10^{-54})$. Nevertheless, several other contributions exist in ALRM models, as illustrated by the other Feynman diagrams in Fig. 6. These diagrams open $\mu \to e\gamma$ decay via the exchange of additional (possibly light) charged Higgs bosons $H_{1,2}^{\pm}$ and charged gauge boson W_R.

The first two diagrams in Fig. 6 contribute to the two form factors $\mathcal{A}_L$ (for diagrams with a W-boson exchanges) and $\mathcal{A}_R$ (for diagrams with a W_R-boson exchange), the corresponding amplitude being given by

$$\mathcal{A}_{\nu_i}^{W_L} = \frac{g_L^2}{2}\frac{em_\mu}{64\pi^2}\frac{1}{M_{W_L}^2}\sum_i \mathcal{V}_{ei}^{\nu\nu}\mathcal{V}_{\mu i}^{\nu\nu*}F_1\left(\frac{m_{\nu_i}^2}{M_{W_L}^2}\right),$$

$$\mathcal{A}_{N_i}^{W_L} = \frac{g_L^2}{2}\frac{em_\mu}{64\pi^2}\frac{1}{M_{W_L}^2}\sum_i \mathcal{V}_{ei}^{\nu N}\mathcal{V}_{\mu i}^{\nu N*}F_1\left(\frac{M_{N_i}^2}{M_{W_L}^2}\right), \tag{31}$$

$$\mathcal{A}_{n_i}^{W_R} = \frac{g_R^2}{2}\frac{em_\mu}{64\pi^2}\frac{1}{M_{W_R}^2}\sum_i \mathcal{V}_{ei}^{nn}\mathcal{V}_{\mu i}^{nn*}F_1\left(\frac{M_{n_i}^2}{M_{W_R}^2}\right),$$

with the loop function

$$F_1(x) = \frac{10 - 43x + 78x^2 - 49x^3 + 18x^3\text{Log}(x) + 4x^4}{6(1-x)^4}. \tag{32}$$

While $\mathcal{A}_{\nu_i}^{W_L}$ is negligible owing to both GIM suppression and the smallness of the light-neutrino masses ($m_\nu \ll M_{W_L}$), we further assume that light-heavy neutrino mixings ($\mathcal{V}^{\nu N}$) are very small (to accommodate neutrino data) so that $\mathcal{A}_{N_i}^{W_L}$ is even more insignificant. On the other hand, the scotino mass can be large, which then cancel any suppression in diagrams exhibiting W_R boson exchanges. By virtue of the properties of the function F_1,

$$F_1(x \to \infty) = \frac{2}{3} + \frac{3\log(x)}{x}, \quad F_1(x \to 0) = \frac{5}{3} - \frac{1}{2}x, \quad F_1(x \to 1) = \frac{17}{12} + \frac{3}{20}(1-x), \tag{33}$$

the relevant amplitude can be simplified according to the mass hierarchy between the scotino and the W_R boson. We

hence have

$$
\begin{aligned}
m_{n_i} \ll M_{W_R} \quad &\to \quad \mathcal{A}_{n_i}^{W_R} = -\frac{g_R^2}{4} \frac{e m_\mu}{64\pi^2} \frac{1}{M_{W_R}^4} \sum_i m_{n_i}^2 \; \mathcal{V}_{ei}^{nn} \mathcal{V}_{\mu i}^{nn*} \\
&\qquad = \frac{g_R^2}{4} \frac{e m_\mu}{64\pi^2} \frac{1}{M_{W_R}^4} \left(\Delta m_{n12}^2 \; \mathcal{V}_{e2}^{nn} \mathcal{V}_{\mu 2}^{nn*} + \Delta m_{n13}^2 \; \mathcal{V}_{e3}^{nn} \mathcal{V}_{\mu 3}^{nn*} \right), \\
m_{n_i} \gg M_{W_R} \quad &\to \quad \mathcal{A}_{n_i}^{W_R} = \frac{3g_R^2}{2} \frac{e m_\mu}{64\pi^2} \sum_i \frac{1}{m_{n_i}^2} \mathrm{Log}\left(\frac{m_{n_i}^2}{M_{W_R}^2} \right) \; \mathcal{V}_{ei}^{nn} \mathcal{V}_{\mu i}^{nn*}, \\
m_{n_i} \sim M_{W_R} \quad &\to \quad \mathcal{A}_{n_i}^{W_R} = -\frac{3g_R^2}{2} \frac{e m_\mu}{1280\pi^2} \frac{1}{M_{W_R}^4} \sum_i m_{n_i}^2 \; \mathcal{V}_{ei}^{nn} \mathcal{V}_{\mu i}^{nn*} \\
&\qquad = \frac{3g_R^2}{40} \frac{e m_\mu}{64\pi^2} \frac{1}{M_{W_R}^4} \left(\Delta m_{n12}^2 \; \mathcal{V}_{e2}^{nn} \mathcal{V}_{\mu 2}^{nn*} + \Delta m_{n13}^2 \; \mathcal{V}_{e3}^{nn} \mathcal{V}_{\mu 3}^{nn*} \right),
\end{aligned}
\tag{34}
$$

with $\Delta m_{n12}^2 = m_{n_1}^2 - m_{n_2}^2$ and $\Delta m_{n13}^2 = m_{n_1}^2 - m_{n_3}^2$. When the particle spectrum is such that $m_{n_i} \gg M_{W_R}$, all contributions are suppressed by factor of $1/m_{n_i}^2$. This is not the case for other spectrum configurations. In particular, when $m_{n_i} \approx M_{W_R}$, the amplitude could get relatively large, provided that the scotino spectrum is close to being degenerate while exhibiting non-zero mass differences together with not too small mixing matrix elements.

We now turn to the contributions mediated by charged scalars, *i.e.* the last two diagrams in Fig. 6. In this case, the amplitudes can be written in a compact from once the light-heavy neutrino mixing matrix elements $\mathcal{V}_{\alpha i}^{\nu N}$ and $\mathcal{V}_{\alpha i}^{N\nu}$ are neglected,

$$
\begin{aligned}
\mathcal{A}_L^{H_1^\pm} &= \frac{e m_\mu}{8\pi^2} \frac{Y_L^{\mu*} Y_L^e}{M_{H_1^\pm}^2} \frac{k^2}{(k^2+v_L^2)} \sum_i \mathcal{V}_{ei}^{NN} \mathcal{V}_{\mu i}^{NN*} F_2\left(\frac{M_{N_i}^2}{M_{H_1^\pm}^2} \right), \\
\mathcal{A}_R^{H_1^\pm} &= \frac{e m_\mu}{8\pi^2} \frac{Y^\mu Y^{e*}}{M_{H_1^\pm}^2} \frac{v_L^2}{(k^2+v_L^2)} \sum_i \mathcal{V}_{ei}^{\nu\nu} \mathcal{V}_{\mu i}^{\nu\nu*} F_2\left(\frac{m_{\nu_i}^2}{M_{H_1^\pm}^2} \right), \\
\mathcal{A}_L^{H_2^\pm} &= \frac{e m_\mu}{8\pi^2} \frac{Y^{\mu*} Y^e}{M_{H_2^\pm}^2} \frac{v_R^2}{(k^2+v_R^2)} \sum_i \mathcal{V}_{ei}^{nn} \mathcal{V}_{\mu i}^{nn*} F_2\left(\frac{m_{n_i}^2}{M_{H_2^\pm}^2} \right), \\
\mathcal{A}_R^{H_2^\pm} &= \frac{e m_\mu}{8\pi^2} \frac{Y_R^{\mu*} Y_R^e}{M_{H_2^\pm}^2} \frac{k^2}{(k^2+v_R^2)} \sum_i \mathcal{V}_{ei}^{nn} \mathcal{V}_{\mu i}^{nn*} F_2\left(\frac{m_{n_i}^2}{M_{H_2^\pm}^2} \right),
\end{aligned}
\tag{35}
$$

where the scalar function $F_2(x)$ defined in the limit $m_e \ll m_\mu \ll M_{H_{1,2}^\pm}$, m_{n_i}, M_{N_i} is given by

$$
F_2(x) = \frac{1 - 6x + 3x^2 + 2x^3 - 6x^2 \log(x)}{6(1-x)^4}.
\tag{36}
$$

This function takes a simpler form in well-defined limits,

$$
F_2(x \to \infty) = \frac{1}{3x}, \quad F_2(x \to 0) = \frac{1}{6} - x, \quad F_2(x \to 1) = \frac{7}{60} - \frac{x}{30},
\tag{37}
$$

so that the amplitudes driven by charged scalar exchanges only play a role when $M_{H_1^\pm} \approx M_N$ and $M_{H_2^\pm} \approx m_n$. In this case, the left-handed form factors approximately read

$$
\begin{aligned}
\mathcal{A}_L^{H_1^\pm} &\approx \frac{1}{30} \frac{e m_\mu}{8\pi^2} \frac{Y_L^{\mu*} Y_L^e}{M_{H_1^\pm}^4} \left(\Delta M_{N_{12}}^2 \; \mathcal{V}_{e2}^{NN} \mathcal{V}_{\mu 2}^{NN*} + \Delta M_{N_{13}}^2 \; \mathcal{V}_{e3}^{NN} \mathcal{V}_{\mu 3}^{NN*} \right), \\
\mathcal{A}_L^{H_2^\pm} &\approx \frac{1}{30} \frac{e m_\mu}{8\pi^2} \frac{Y^{\mu*} Y^e}{M_{H_2^\pm}^4} \left(\Delta m_{n_{12}}^2 \; \mathcal{V}_{e2}^{nn} \mathcal{V}_{\mu 2}^{nn*} + \Delta m_{n_{13}}^2 \; \mathcal{V}_{e3}^{nn} \mathcal{V}_{\mu 3}^{nn*} \right),
\end{aligned}
\tag{38}
$$

and we do not provide expressions for the right-handed form factors as they turn out be be negligible for the parameter space considered in our analysis.

In order to quantitatively assess the impact of these different contributions, we perform a numerical analysis exploring the different mass configurations sketched in Eqs. (34) and (38). For this purpose, we implement a scan of the parameter space with the input parameters specified in Eqs. (17) and (18). With $\tan\beta$ varying in the given range, $v_L \ll k$ so that contributions from $A_R^{H_1^\pm}$ are negligible, and $k \ll v_R$ so that $A_R^{H_2^\pm}$ is equally small, as already mentioned above. We can note that the impact of these contributions was already quite mild due to the smallness of m_ν and the corresponding approximate GIM suppression. Non-zero and significant contributions to the $\mu \to e\gamma$ LFV decay therefore arise predominantly from diagrams involving a left-handed muon.
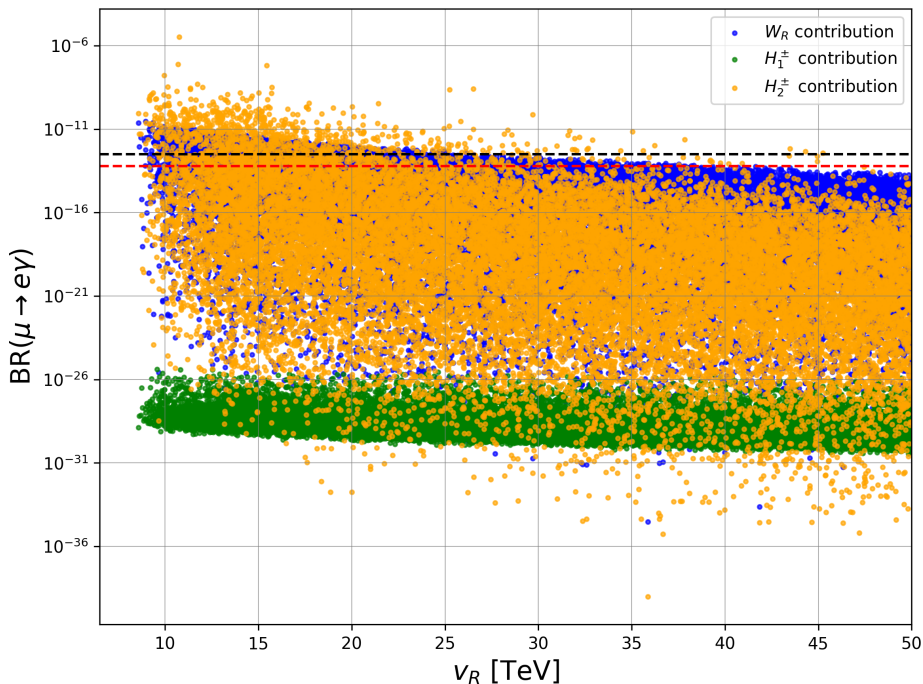
FIG. 7: Distributions of the contributions to $\mathrm{BR}(\mu \to e\gamma)$ from W_R/n_i (blue), $H_1^\pm/N_i$ (green) and $H_2^\pm/n_i$ (orange) exchanges, presented as a function of v_R. The horizontal dashed lines represent current bounds (black) and the future sensitivity (red) on this branching ratio, as expected from the MEG II experiment [73, 74]. Only predictions for scenarios in which $M_{Z'} > 4.5$ TeV are displayed.
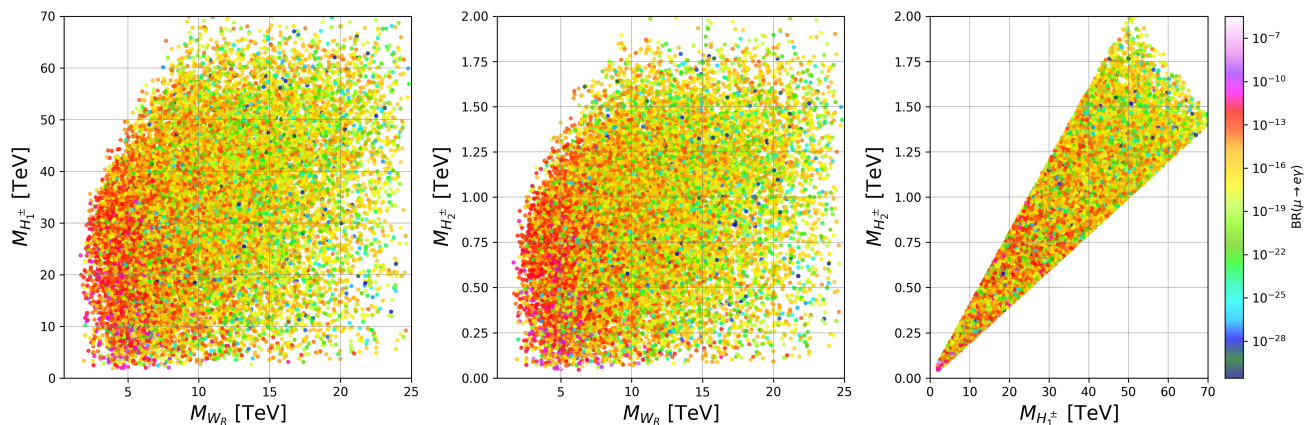

FIG. 8: Predictions of the $\mathrm{BR}(\mu \to e\gamma)$ branching ratio in the ALRM, shown within varied two-dimensional mass planes defined by the W_R, $H_1^\pm$ and $H_2^\pm$ masses.

In Fig. 7 we present predictions for the various contributions to $\mathrm{BR}(\mu \to e\gamma)$, while separating the individual channels, and we depict their dependence on v_R. From all scanned points, we only retain those where the Z' boson is heavy enough to evade collider bounds, *i.e.* with $M_{Z'} > 4.5$ TeV. Contributions from W_R/scotino exchanges, $H_1^\pm$/heavy neutrino exchanges and $H_2^\pm$/scotino exchanges are shown in blue, green and orange, respectively. Given that $M_{H_1^\pm}^2 \sim \tan\beta M_{H_2^\pm}^2$ for the scanned region of the parameter space, the first Higgs mass $M_{H_1^\pm}$ is always about an order or magnitude larger than the mass of the second Higgs state $M_{H_2^\pm}$. Therefore, contributions featuring $H_1^\pm$ mediation are expected to be much smaller than those mediated by $H_2^\pm$ exchanges. This is clearly illustrated in Fig. 7, which shows that $H_2^\pm$ contributions to $\mathrm{BR}(\mu \to e\gamma)$ can often be a few orders of magnitude larger than those involving $H_1^\pm$. Furthermore, despite the very large W_R boson mass, the associated contributions are always large by virtue of the couplings involved and often of similar size as those emerging from exchanges of the much lighter $H_2^\pm$ Higgs boson.
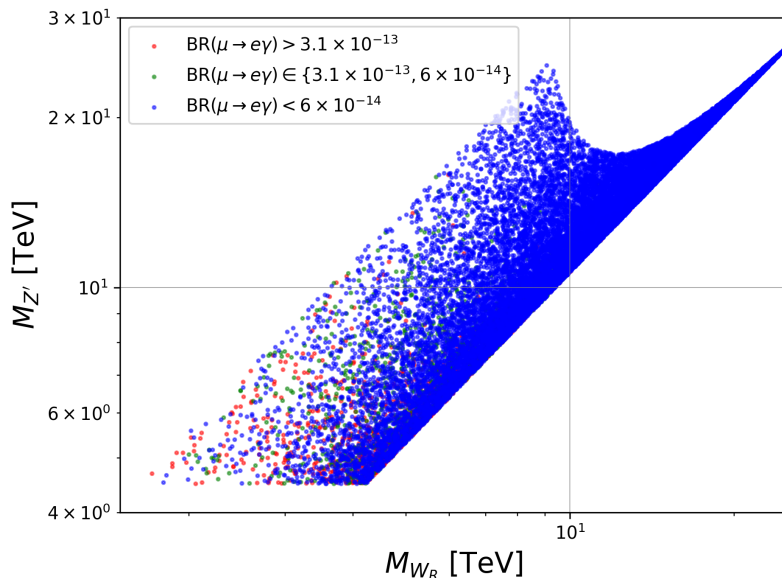
FIG. 9: Allowed regions of the scanned parameter space projected in the $(M_{W_R}, M_{Z'})$ plane. We distinguish scenarios only allowed by current LHC bounds on the Z' boson with $M_{Z'} > 4.5$ TeV but excluded by current MEG II measurement (red), scenarios that feature $\mathrm{BR}(\mu \to e\gamma) \in \{3.1 \times 10^{-13}, 6 \times 10^{-14}\}$ (green), and finally scenarios such that $\mathrm{BR}(\mu \to e\gamma) < 6 \times 10^{-14}$ (blue).

We recall that throughout our parameter scan, the charged scalar $H_2^{\pm}$ is often found to be light, with a mass being one order of magnitude smaller than that of the W_R boson. The charged Higgs contribution to the branching ratio $\mathrm{BR}(\mu \to e\gamma)$ is consequently relatively enhanced. However, the $SU(2)_{R'}$ gauge coupling is always stronger than the small neutrino/scotino Yukawa couplings relevant for the charged Higgs contributions in the model considered. These W_R-boson exchange contributions are thus often by themselves sufficient to exclude a given scenario (as are those mediated by the second charged Higgs), or will soon be, as testified by the black and the red dashed lines representing the current and future bounds on the $\mu \to e\gamma$ branching ratio from the MEG II experiment [73, 74].

In Fig. 8, we display predictions (summed over all diagrams) for the (total) branching ratio $\mathrm{BR}(\mu \to e\gamma)$ through a colour code, all scanned points being projected in three different two-dimensional mass planes. In the left and central panels of the figure, we consider the $(M_{W_R}, M_{H_1^{\pm}})$ and $(M_{W_R}, M_{H_2^{\pm}})$ mass planes respectively, while in the rightmost panel we present the results in the $(M_{H_1^{\pm}}, M_{H_2^{\pm}})$ plane. As just mentioned, for the whole range of values spanned by the v_R parameter in our scan, diagrams featuring W_R and $H_2^{\pm}$ boson exchanges yield the dominant contributions to the rare branching ratio, and those contributions are generally of the same order. The main difference arises from the masses of the two bosons, which is highlighted in the different panels of Fig. 8. For scenarios with a light W_R state with $M_{W_R} \lesssim 10$ TeV, $\mathrm{BR}(\mu \to e\gamma)$ is generally the largest with branching ratio values often greater than 10^{-12}, regardless of the mass of the second charge Higgs that could be equally below or above 1 TeV. For heavier W_R boson with mass larger than 10 TeV, the branching ratio drops by several orders of magnitude. The connection between the mass of the second charged Higgs and that of the W_R boson prevents the $H_2^{\pm}$ boson contributions to be large enough to compensate for this drop. Finally, we recall that the charged Higgs masses are strongly correlated, as mentioned above, and as shown in the right panel of the figure.

We close this section by presenting in Fig. 9, the regions of the parameter space allowed by current LHC bounds on the ALRM Z' state, and that could be further restricted by present bounds and future sensitivity on the rare branching ratio $\mathrm{BR}(\mu \to e\gamma)$. All scanned scenarios satisfying LHC bounds on the Z' boson (i.e., with $M_{Z'} > 4.5$ TeV) are projected in the two-dimensional mass plane $(M_{W_R}, M_{Z'})$. Such a representation allows us to determine, by means of the relationship between the extra gauge boson masses, how constraints on the W_R boson from rare $\mu \to e\gamma$ decays could provide information on bounds on the neutral Z' boson. All the points that are excluded by current MEG II measurement on the branching ratio $\mathrm{BR}(\mu \to e\gamma)$ are shown in red, whilst those which are sensitive to MEG II present bound but will be disfavoured in the near future are shown in green. Finally, blue points refer to scenarios featuring a too small $\mathrm{BR}(\mu \to e\gamma)$ value to be reachable by any planned experiment. We can infer from this figure that indirect LFV constraints have the potential to restrict the viable regions of the parameter space further, or equivalently that constraints could be extracted on the W_R mass from improved measurements of the rare branching ratio $\mathrm{BR}(\mu \to e\gamma)$. Subsequently, there is a potential to increase mass bounds on the ALRM Z' boson beyond those originating from the

LHC, owing to the band-like structure which appears in the plane and that is due to varying the g_R coupling in our scan and the sensitivity to $\text{BR}(\mu \to e\gamma)$. Finally, we emphasise that the specific shape of the upper-right boundary of the parameter space region populated by the points directly arises from the quadratic tree-level relationship between the Z' and W_R masses, combined with the LHC mass limits imposed by Z' boson searches at the LHC.

B. $\mu - e$ conversion in nuclei

In this section we analyse the impact of a typical ARLM spectrum on $\mu - e$ conversion in nuclei, which consists in one of the most promising experimental projects to test lepton flavour violation in the future. It has therefore attracted a lot of phenomenological interest for more than 50 years [87–95]. The summary of the current experimental status on the conversion rate for $\mu - e$ processes in aluminium, titanium and gold is presented in the second column of Table II. Furthermore, these constraints are expected to be improved by several orders of magnitude in the near future, as shown in the third column of the table that collects expectations of experiments such as DeeMe at J-PARC [96] with its expected sensitivity of $\mathcal{O}(10^{-14})$, Mu2e at Fermilab [97] with an expected sensitivity of $\mathcal{O}(10^{-17})$, and COMET at J-PARC [98] with a $\mathcal{O}(10^{-15})$ sensitivity in its first phase and $\mathcal{O}(10^{-17})$ in its second phase. These low bounds make $\mu - e$ conversions very attractive for constraining models featuring non-standard lepton-flavor-violating interactions like the ALRM.

In nuclei, $\mu - e$ conversions are traditionally studied within an effective field theory approach [90, 99]. This effective description relies on a parton-level Lagrangian embedding higher-dimensional interactions between light quark ($q = u, d, s$), electron (e) and muon (μ) fields,

$$-\mathcal{L}_{\text{eff}}^{(q)} \subset -\sqrt{2}G_F \left[\sum_{X=L,R} \left(C_{DX} m_\mu (\bar{e}\sigma^{\alpha\beta} P_X \mu) F_{\alpha\beta} + C_{GX} \frac{\alpha_s}{4\pi} \frac{m_\mu}{v^2} (\bar{e} P_X \mu) G_{a\alpha\beta} G^{a\alpha\beta} \right) \right.$$
$$\left. + \sum_{q=u,d,s} \sum_{X,Y=L,R} \left(C_{VXY}^{(q)} (\bar{e}\gamma^\alpha P_X \mu)(\bar{q}\gamma_\alpha P_Y q) + C_{SXY}^{(q)} (\bar{e} P_X \mu)(\bar{q} P_Y q) \right) + \text{H.c.} \right]. \tag{39}$$

In this Lagrangian, the Wilson coefficients C_{DX}, C_{GX}, $C_{VXY}^{(q)}$ and $C_{SXY}^{(q)}$ encode the UV dynamics of the theory (with $X, Y = L, R$), and they are thus dependent on the model considered. They can be related in a second step to coefficients encoding the nucleon-level dynamics. To bridge the gap between the parton and nucleon regimes, we follow the methodology outlined in Refs. [90, 92]. We extract proton-level and neutron-level effective coefficients,

$$\widetilde{C}_{VX}^{(p)} = \sum_{q_k=u,d,s} \sum_{Y=L,R} C_{VXY}^{(q)} f_{Vp}^{(q_k)},$$
$$\widetilde{C}_{VX}^{(n)} = \sum_{q_k=u,d,s} \sum_{Y=L,R} C_{VXY}^{(q)} f_{Vn}^{(q_k)},$$
$$\widetilde{C}_{SX}^{(p)} = \sum_{q_K=u,d,s} \sum_{Y=L,R} \frac{m_p}{m_q} C_{SXY}^{(q)} f_{Sp}^{(q_k)} + \frac{m_\mu m_p}{4\pi v^2} C_{G_X} f_{Gp}, \tag{40}$$
$$\widetilde{C}_{SX}^{(n)} = \sum_{q_K=u,d,s} \sum_{Y=L,R} \frac{m_p}{m_q} C_{SXY}^{(q)} f_{Sn}^{(q_k)} + \frac{m_\mu m_p}{4\pi v^2} C_{G_X} f_{Gn},$$

where the various f coefficients are the conventional nucleon, scalar and gluonic form factors [100, 101],

$$f_{Vp}^{(u)} = 2, \qquad f_{Vp}^{(d)} = 1, \qquad f_{Vp}^{(s)} = 0, \qquad f_{Vn}^{(u)} = 1, \qquad f_{Vn}^{(d)} = 2, \qquad f_{Vp}^{(s)} = 0,$$
$$f_{Sp}^{(u)} = (20.8 \pm 1.5) \times 10^{-3}, \qquad f_{Sp}^{(d)} = (41.1 \pm 2.8) \times 10^{-3}, \qquad f_{Sp}^{(s)} = (53.0 \pm 27) \times 10^{-3},$$
$$f_{Sn}^{(u)} = (18.9 \pm 1.4) \times 10^{-3}, \qquad f_{Sn}^{(u)} = (45.1 \pm 2.7) \times 10^{-3}, \qquad f_{Sn}^{(s)} = (53.0 \pm 27) \times 10^{-3}, \tag{41}$$
$$f_{Gp(n)} = -\frac{8\pi}{9} \left[1 - \sum_{q=u,d,s} f_{Sp(n)}^{(q)} \right].$$

The $\mu \to e$ conversion rate normalised to the muon capture rate Γ_{capt} in a specific nucleus N is then given by [90]

$$\text{CR}(\mu - e)(N) = \frac{m_\mu^5}{4\Gamma_{\text{capt}}(N)} \left| C_{DL} D_N + 2\left[\widetilde{C}_{(p)}^{VR} V_N^{(p)} + \widetilde{C}_{(p)}^{SL} S_N^{(p)} + (p \to n) \right] \right|^2 + (L \leftrightarrow R), \tag{42}$$

where the dimensionless integrals D_N and $V_N^{(q)}$ represent the overlap between the electron and muon wave functions. Explicit expressions for these integrals can be found in Refs. [89, 90], and the muon capture rate $\Gamma_{\text{capt}}(N)$ by a nucleus

Isotope	D_N [90]	$V^{(p)}$ [90]	$V^{(n)}$ [90]	$S^{(p)}$ [102]	$S^{(n)}$ [102]	$\Gamma_{\mathrm{capt}}(10^6 \text{ s}^{-1})$ [103]
$^{27}_{13}\mathrm{Al}$	0.0359	0.0165	0.0178	0.0159	0.0172	0.69
$^{48}_{22}\mathrm{Ti}$	0.0859	0.0407	0.0481	0.0379	0.0448	2.59
$^{127}_{79}\mathrm{Au}$	0.1660	0.0866	0.1290	0.0523	0.0781	13.07

TABLE III: Numerical values for the nuclear physics inputs and muon capture rates in different isotopes, that are relevant for the calculation of $\mu - e$ conversion rates performed in this work.

FIG. 10: Feynman diagrams driving $\mu - e$ conversion processes in nuclei in ALRM scenarios. The two top (bottom) leftmost diagrams represent contributions from $W_R^\pm$ ($W_L^\pm$) -boson exchanges, while the two top (bottom) rightmost diagrams are related to contributions from $H_2^\pm$ ($H_1^\pm$) exchanges.

N with atomic and mass numbers Z and A is related to the cross section associated with the process

$$\mu^- + (Z, A) \to \nu_\mu + (Z - 1, A), \qquad \text{or equivalently} \qquad \mu^- + p \to \nu_\mu + n. \tag{43}$$

Numerical values for all relevant nuclear physics inputs appearing in Eq. (42) are available from [90, 102, 103], and we collect them in Table III.

In the ALRM and at one loop, $\mu - e$ conversions solely arise from triangle contributions, since any potential box diagram involves joint W_L-boson and $H_1^\pm$-boson exchanges and is therefore vanishing. The relevant Feynman diagrams are shown in Fig. 10. In the following, we mainly focus on t-channel photonic exchanges, because diagrams featuring mediation via a heavy neutral gauge boson are suppressed by a massive vector propagator, at least when compared with diagrams including a massless photon propagator. We are thus left to estimate the impact of few remaining diagrams on the Wilson coefficients appearing in the Lagrangian of Eq. (39).

We perform our computations in the elastic limit, as typical momentum transfers given by $t = (p_{(\mu)} - p_{(e)})^2$ are of the order of m_μ^2. In contrast to the computations relevant for $\mu \to e\gamma$ decays that we have addressed in the previous section, the photon appearing in the muon conversion diagrams is off-shell. The limit $t \to 0$ can thus be safely taken, especially as $m_\mu^2 \sim 0$ relatively to the large masses of the charged bosons running into the loops. Considering this limit as well as negligible light-heavy neutrino mixing ($V^{\nu N}, V^{N\nu}$); several Wilson coefficients of Eq. (39) are modified
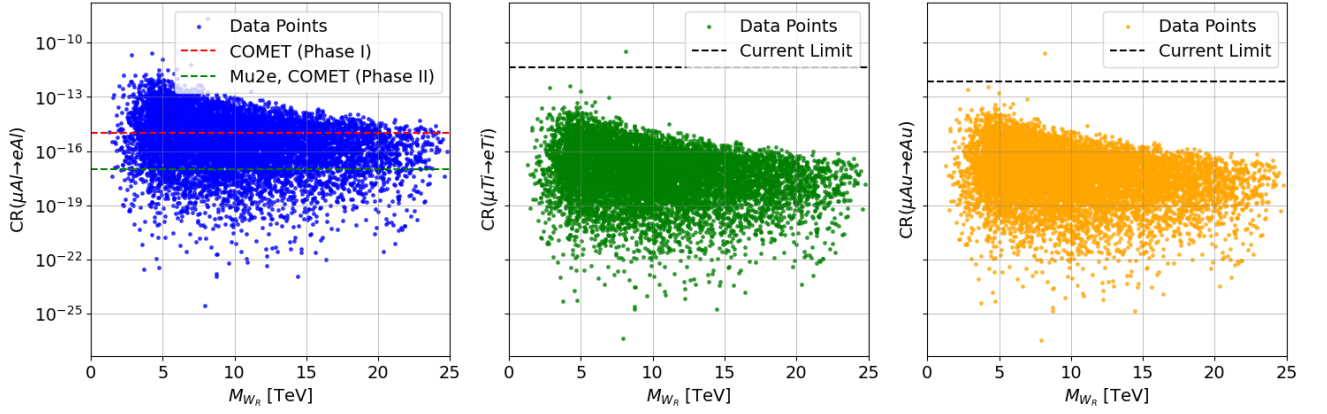
FIG. 11: Muon capture rates in Al (left), Ti (centre) and Au (right) as returned by our scan of the ALRM parameter space, and displayed as a function of the W_R boson mass. The sensitivities of several current and future experiments are indicated through dashed horizontal lines. Here we have imposed the experimental constraint of $M_{Z'} > 4.5$ TeV while scanning the parameter space.

by ALRM effects,

$$C_{DL}(H_1^{\pm}) = \frac{e}{16\pi^2} \frac{1}{M_{H_1^{\pm}}^2} \left[Y_L^{\mu*} Y_L^e \frac{k^2}{k^2+v_L^2} \right] \sum_i V_{\mu i}^{NN*} V_{\mu i}^{NN} F_2 \left(\frac{M_{N_i}^2}{M_{H_1^{\pm}}^2} \right),$$

$$C_{DR}(H_1^{\pm}) = \frac{e}{16\pi^2} \frac{1}{M_{H_1^{\pm}}^2} \left[Y^{\mu*} Y^e \frac{v_L^2}{k^2+v_L^2} \right] \sum_i V_{\mu i}^{\nu\nu*} V_{\mu i}^{\nu\nu} F_2 \left(\frac{m_{\nu_i}^2}{M_{H_1^{\pm}}^2} \right),$$

$$C_{DL}(H_2^{\pm}) = \frac{e}{16\pi^2} \frac{1}{M_{H_2^{\pm}}^2} \left[Y^{\mu*} Y^e \frac{v_R^2}{(k^2+v_R^2)} \right] \sum_i \mathcal{V}_{\mu i}^{nn*} \mathcal{V}_{ei}^{nn} F_2 \left(\frac{M_{n_i}^2}{M_{H_2^{\pm}}^2} \right),$$

$$C_{DR}(H_2^{\pm}) = \frac{e}{16\pi^2} \frac{1}{M_{H_2^{\pm}}^2} \left[Y_R^{\mu*} Y_R^e \frac{k^2}{(k^2+v_R^2)} \right] \sum_i \mathcal{V}_{\mu i}^{nn*} \mathcal{V}_{ei}^{nn} F_2 \left(\frac{M_{n_i}^2}{M_{H_2^{\pm}}^2} \right),$$

$$C_{DL}(W_L^{\pm}) = \frac{e}{64\pi^2} \frac{1}{M_{W_L^{\pm}}^2} \frac{g_L^2}{4} \sum_i V_{\mu i}^{\nu\nu*} V_{ei}^{\nu\nu} F_1 \left(\frac{m_{\nu_i}^2}{M_{W_L^{\pm}}^2} \right),$$

$$C_{DR}(W_R^{\pm}) = \frac{e}{64\pi^2} \frac{1}{M_{W_R^{\pm}}^2} \frac{g_R^2}{4} \sum_i \mathcal{V}_{\mu i}^{nn*} \mathcal{V}_{ei}^{nn} F_1 \left(\frac{M_{n_i}^2}{M_{W_R^{\pm}}^2} \right), \tag{44}$$

the contributions to the other coefficients being either exactly zero (like for the vector coefficient $C_{VRR}^{(q)}$) or suppressed by the small size of the neutrino masses and related couplings (like for $C_{VLL}^{(q)}$, $C_{VLR}^{(q)}$ and $C_{VRL}^{(q)}$), heavy neutral scalar propagators (like for scalar coefficients) or the smallness of the scalar form factors f_{Si} in Eq. (41), compared to the order of magnitude of the other form factors. We refer to the discussion in Ref. [104] for comprehensive details on the different contributions to muon conversions in left-right models. Among all the contributions, the triangle diagrams exhibiting W_L and $H_1^{\pm}$ boson exchanges are negligible due to GIM suppression and the smallness of the light-neutrino masses ($m_\nu \ll M_{W_L}, M_{H_1^{\pm}}$). Moreover, contributions arising from the exchange of $H_1^{\pm}$ charged Higgs bosons are significantly further suppressed due to its mass. The large mass of the $H_1^{\pm}$ boson indeed leads to suppression in the corresponding propagators, thus reducing the overall impact of these contributions on the relevant processes. Therefore, the only relevant contributions come from the Feynman diagrams mediated by W_R-boson and $H_2^{\pm}$-boson exchanges.

In Fig. 11 we compare our predictions to bounds on $\mu - e$ conversion stemming from current measurements, and to expectations for the sensitivity of several future experiments. We scan over the parameter space following the inputs specified in Eqs. (17) and (18), and for each point we evaluate the muon capture rate in aluminium (left), titanium (centre) and gold (right) as a function of W_R mass. We observe that mild bounds on the ALRM parameter space already exist, from achieved measurements, but that future experiments have the potential to strongly restrict the phenomenologically viable part of the parameter space. This is particularly pronounced for muon capture in aluminium, where future measurements have the potential to yield stringent constraints on ALRM scenarios with a
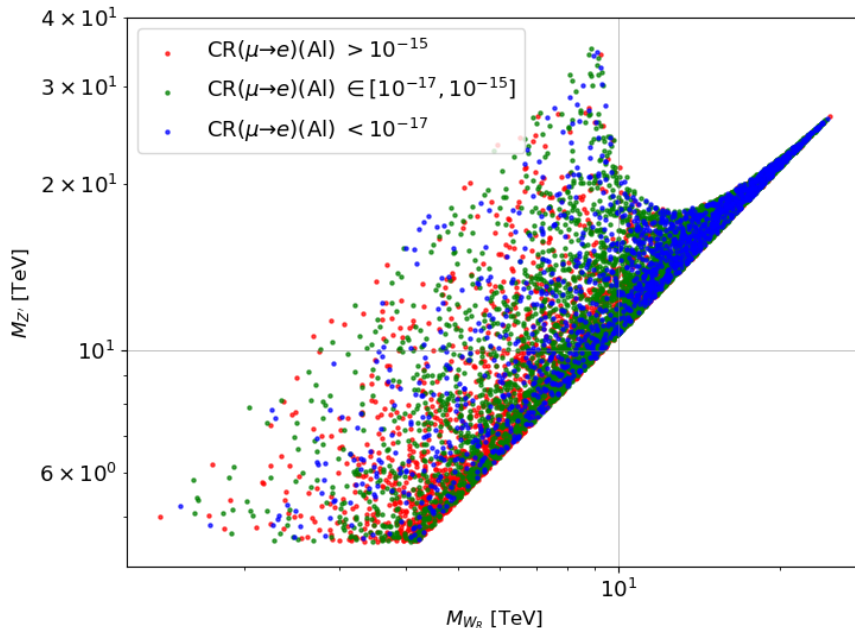
FIG. 12: Muon capture rates in Al, projected in the two-dimensional mass plane $(M_{W_R}, M_{Z'})$. We display predictions for all scenarios explored in our scan, the colour code indicating whether a given scenario has the potential to be probed in the future at COMET-I (red), and at Mu2e and COMET-II (green), or the predictions are such that the scenario is not reachable at any future planned experiment (blue). Here we have imposed the experimental constraint of $M_{Z'} > 4.5$ TeV while scanning the parameter space.

charged vector boson mass $M_{W_R} \geq 1300$ GeV and drastically reduce the range of acceptable possibilities.

Finally, we explore the potential of using the existing correlation between the W_R-boson and Z'-boson masses to indirectly constrain the properties of ALRM Z' boson via W_R contributions to $\mu - e$ transitions in nuclei. To this aim, we project in Fig. 12 all points of our scan in the $(M_{W_R}, M_{Z'})$ mass plane, focusing on conversions in aluminium, as only this nucleus has the potential to constrain the ALRM (as shown in Fig. 11). Our findings show that a large class of scenarios featuring a Z' boson with mass lying between 5 and 35 TeV have the potential to be excluded for $M_{W_R} \lesssim 12$ TeV (and even in the heaviest Z' setups). However, many scenarios will still remain beyond the reach of present and future experiments for all values of the W_R boson mass (and all corresponding values of the Z'-boson mass), the associated contributions being not large enough to provide any substantial enhancement. Consequently, while indirect $\mu - e$ conversion constraints will strengthen our knowledge of which ALRM configuration will remain phenomenologically acceptable in a close future, existing conspiracy between the numerous free parameters of the model (in particular v_R and g_R) will hinder our ability to draw a generic conclusion on the possible masses for the extra charged and neutral gauge bosons.

V. CONCLUSION

We explored an alternative version of the left-right symmetric model emerging from a grand unified theory that embeds a gauge symmetry based on the exceptional E_6 group. The breaking of this symmetry group to the electroweak symmetry group yields an intermediate left-right symmetry pairing the SM fermions with exotic down-type quark and neutrino states, the latter being dubbed scotinos. Moreover, the symmetry breaking pattern originates from the presence of an enriched Higgs sector featuring several neutral and charged physical Higgs bosons. In this work, we assess how this spectrum of extra fields has the potential to impact several leptonic observables, and how existing and future associated measurements have the potential to constrain the model. Very interestingly, in the ALRM the W_R boson is only constrained at colliders indirectly, through the relationship between its mass and the extra neutral boson Z'. Conversely, we investigate how indirect probes from leptonic observables on the W_R boson could bring complementary information.

We chose the focus first on the anomalous magnetic moment of the muon, and we demonstrated by means of a vast scan of the model parameter space that ALRM scenarios have little chance to contribute largely enough to explain the

Interaction	Vector (g_V)	Axial-vector (g_A)
$\bar{\ell}_i\ell_i Z$	$i\left[-\frac{eg_L}{2g_Y}+\frac{3eg_Y}{2g_L}\right]$	$i\left[\frac{eg_L}{2g_Y}+\frac{eg_Y}{2g_L}\right]$
$\bar{\ell}_i\ell_i Z'$	$i\frac{-g_R^2+3g_Y^2}{2\sqrt{g_R^2-g_Y^2}}$	$i\frac{-g_R^2+g_Y^2}{2\sqrt{g_R^2-g_Y^2}}$
$\bar{\ell}_j\nu_i W_L^-$	$i\frac{g_L}{2\sqrt{2}}\mathcal{V}_{ji}^{\nu\nu}$	$-i\frac{g_L}{2\sqrt{2}}\mathcal{V}_{ji}^{\nu\nu}$
$\bar{\ell}_j N_i W_L^-$	$i\frac{g_L}{2\sqrt{2}}\mathcal{V}_{ji}^{\nu N}$	$-i\frac{g_L}{2\sqrt{2}}\mathcal{V}_{ji}^{\nu N}$
$\bar{\ell}_j n_i W_R^-$	$i\frac{g_R}{2\sqrt{2}}\mathcal{V}_{ji}^{nn*}$	$i\frac{g_R}{2\sqrt{2}}\mathcal{V}_{ji}^{nn*}$

Interaction	Scalar (g_S)	Pseudo-scalar (g_P)
$\bar{\ell}_i\ell_i h$	$-iY_{ii}^\ell U_{11}^H$	0
$\bar{\ell}_i\ell_i H_2^0$	$-iY_{ii}^\ell U_{12}^H$	0
$\bar{\ell}_i\ell_i H_3^0$	$-iY_{ii}^\ell U_{13}^H$	0
$\bar{\ell}_i\ell_i A_2^0$	0	$Y_{ii}^\ell U_{13}^A$
$\bar{\ell}_j\nu_i H_1^-$	$i\frac{Y_{kj}^\ell \mathcal{V}_{ki}^{\nu\nu} v_L + Y_{L,jk}^\ell \mathcal{V}_{ki}^{\nu N} k}{\sqrt{k^2+v_L^2}}$	$i\frac{-Y_{kj}^\ell \mathcal{V}_{ki}^{\nu\nu} v_L + Y_{L,jk}^\ell \mathcal{V}_{ki}^{\nu N} k}{\sqrt{k^2+v_L^2}}$
$\bar{\ell}_j N_i H_1^-$	$i\frac{Y_{kj}^\ell \mathcal{V}_{ki}^{N\nu} v_L + Y_{L,jk}^\ell \mathcal{V}_{ki}^{NN} k}{\sqrt{k^2+v_L^2}}$	$i\frac{-Y_{kj}^\ell \mathcal{V}_{ki}^{N\nu} v_L + Y_{L,jk}^\ell \mathcal{V}_{ki}^{NN} k}{\sqrt{k^2+v_L^2}}$
$\bar{\ell}_j n_i H_2^-$	$i\frac{\mathcal{V}_{ki}^{nn}(Y_{jk}^\ell v_R + Y_{R,jk} k)}{\sqrt{k^2+v_R^2}}$	$i\frac{\mathcal{V}_{ki}^{nn}(Y_{jk}^\ell v_R - Y_{R,jk} k)}{\sqrt{k^2+v_R^2}}$

TABLE IV: FFV and FFS interactions of massive gauge and Higgs bosons with leptons, the coupling strengths being split into their vector/scalar (g_V/g_A, second column) and axial-vector/pseudu-scalar (g_A/g_P, third column) components. The indices i and j refer to generation indices.

longstanding deviations between the SM predictions and measurements. We calculated one-loop ALRM contributions, that are suppressed due to the relatively high masses of new bosons as compared to the muon mass, as well as the two-loop ones, that suffer from a conspiracy involving the smallness of the relevant Yukawa couplings and the masses of the new fermions running into the loops to keep the full contribution small across the entire parameter space. The negligible ALRM impact on the anomalous magnetic moment of the muon, however, gels well with the most recent lattice results, that advocate agreement between SM and data.

On the other hand, we studied two classes of lepton-flavour-violating processes, namely muon-to-electron conversion in nuclei and muon decays to an electron-photon system. We determined how predictions are impacted in the ALRM at one loop. We perform a general scan of the parameter space, and demonstrated the potential of future related measurements to constrain the masses of the charged Higgs and gauge bosons of the model. Both present and future experimental data have hence the potential to restrict ALRM scenarios featuring a W_R-boson mass larger than 1.3 TeV (from $\mu - e$ conversion in Al), and a charged Higgs masses for scenarios featuring both light and heavy states.

These results are complementary to the mass bounds expected to be obtained at colliders, where the W_R and charged Higgs bosons cannot be directly produced. Present bounds and future sensitivity from MEG II can constrain the Z' mass parameter space more tightly as compared to LHC bounds, but a quantitative limit is difficult to state since the W_R and Z' masses depend on both v_R and g_R parameters which can be varied independently. Hence here we have performed calculations offering the possibility to alternatively constrain the model, even in case where the masses are much larger than existing collider energies.

Acknowledgements

Appendix A: ALRM Couplings to Scalars and Vectors

In this appendix, we list the relevant couplings used in the calculations presented in this paper, as extracted from the Lagrangian introduced in Section II. Table IV collects the fermion-fermion-vector (FFV) and fermion-fermion-scalar (FFS) couplings involving the lepton sector and entering the one-loop contributions to the observables considered. These couplings depend on the electromagnetic, $SU(2)_L$, $SU(2)_{R'}$ and hypercharge gauge couplings e, g_L, g_R and g_Y, as well as on the Yukawa couplings, VEVs and mixing matrices defined in Section II.

In the rest of this section, we focus on the interactions relevant for the two-loop ALRM contributions to the anomalous magnetic moment of the muon, Δa_μ. The couplings relevant for diagram (1) in Fig. 4 include the FFS couplings of Table IV involving a neutral Higgs boson, as well as the FFS couplings to SM top and bottom quarks and to exotic $q'_d = d', s', b'$ quarks given in Table V. These quark couplings are again split in their scalar and pseudo-scalar components, and written in terms of the Yukawa couplings and mixing matrices introduced in Section II. Diagram (2)

Interaction	Scalar (g_S)	Pseudo-scalar (g_P)
$\bar{t}th$	$-iY_{33}^q U_{11}^H$	0
$\bar{t}tH_2^0$	$-iY_{33}^q U_{12}^H$	0
$\bar{t}tH_3^0$	$-iY_{33}^q U_{13}^H$	0
$\bar{t}tA_2^0$	0	$-Y_{33}^q U_{13}^A$

Interaction	Scalar (g_S)	Pseudo-scalar (g_P)
$\bar{b}bh$	$-iY_{L,33}^q U_{21}^H$	0
$\bar{b}bH_2^0$	$-iY_{L,33}^q U_{22}^H$	0
$\bar{b}bH_3^0$	$-iY_{L,33}^q U_{23}^H$	0
$\bar{b}bA_2^0$	0	$-Y_{L,33}^q U_{23}^A$

Interaction	Scalar (g_S)	Pseudo-scalar (g_P)
$\bar{q}'_{d,i} q'_{d,i} h$	$-iY_{R,ii}^q U_{31}^H$	0
$\bar{q}'_{d,i} q'_{d,i} H_2^0$	$-iY_{R,ii}^q U_{32}^H$	0
$\bar{q}'_{d,i} q'_{d,i} H_3^0$	$-iY_{R,ii}^q U_{33}^H$	0
$\bar{q}'_{d,i} q'_{d,i} A_2^0$	0	$-Y_{R,ii}^q U_{33}^A$

TABLE V: As in Table IV, but for the FFS interactions involving SM and exotic quarks and contributing at two loops to Δa_μ. The index i is a generation index.

Interaction	Coupling
$H_1^+ H_1^- h$	$\dfrac{i[-4k^3 U_{11}^H \alpha - 4v_L^3 U_{21}^H \alpha - 4v_L^2 v_R U_{31}^H \alpha - 2k^2 v_L U_{11}^H \lambda_1 - 2k^2 v_L U_{21}^H \lambda_3 - 2k^2 v_R U_{31}^H \lambda_4 + \sqrt{2} k v_L U_{31}^H \kappa]}{(k^2 + v_L^2)}$
$H_1^+ H_1^- H_2^0$	$\dfrac{i[-4k^3 U_{12}^H \alpha - 4v_L^3 U_{22}^H \alpha - 4v_L^2 v_R U_{32}^H \alpha - 2k^2 v_L U_{12}^H \lambda_1 - 2k^2 v_L U_{22}^H \lambda_3 - 2k^2 v_R U_{32}^H \lambda_4 + \sqrt{2} k v_L U_{32}^H \kappa]}{(k^2 + v_L^2)}$
$H_1^+ H_1^- H_3^0$	$\dfrac{i[-4k^3 U_{13}^H \alpha - 4v_L^3 U_{23}^H \alpha - 4v_L^2 v_R U_{33}^H \alpha - 2k^2 v_L U_{13}^H \lambda_1 - 2k^2 v_L U_{23}^H \lambda_3 - 2k^2 v_R U_{33}^H \lambda_4 + \sqrt{2} k v_L U_{33}^H \kappa]}{(k^2 + v_L^2)}$
$H_2^+ H_2^- h$	$\dfrac{i[-4k^3 U_{11}^H \alpha - 4v_L v_R^2 U_{21}^H \alpha - 4v_R^3 U_{31}^H \alpha - 2k v_R^2 U_{11}^H \lambda_1 - 2k^2 v_R U_{31}^H \lambda_3 - 2k^2 v_L U_{21}^H \lambda_4 + \sqrt{2} k v_R U_{21}^H \kappa]}{(k^2 + v_R^2)}$
$H_2^+ H_2^- H_2^0$	$\dfrac{i[-4k^3 U_{12}^H \alpha - 4v_L v_R^2 U_{22}^H \alpha - 4v_R^3 U_{32}^H \alpha - 2k v_R^2 U_{12}^H \lambda_1 - 2k^2 v_R U_{32}^H \lambda_3 - 2k^2 v_L U_{22}^H \lambda_4 + \sqrt{2} k v_R U_{22}^H \kappa]}{(k^2 + v_R^2)}$
$H_2^+ H_2^- H_3^0$	$\dfrac{i[-4k^3 U_{13}^H \alpha - 4v_L v_R^2 U_{23}^H \alpha - 4v_R^3 U_{33}^H \alpha - 2k v_R^2 U_{13}^H \lambda_1 - 2k^2 v_R U_{33}^H \lambda_3 - 2k^2 v_L U_{23}^H \lambda_4 + \sqrt{2} k v_R U_{23}^H \kappa]}{(k^2 + v_R^2)}$
$H_i^+ H_i^- A_2^0$	0

TABLE VI: SSS couplings appearing in the two-loop contributions to Δa_μ.

involves additional trilinear scalar interactions (SSS) that we provide in Table VI, and diagram (3) involves the charged-current gauge interactions of the model's Higgs bosons (VVS) that we display in Table VII, along with the lepton-scalar couplings already introduced in Table IV. Diagrams (4a) and (4b) depend on the FFV and FFS couplings of IV, the SSS couplings of Table VI, and the VSS couplings of Table VII, while diagrams (5a) and (5b) involve the FFS and FFV couplings of Table IV, and the VVS and SSV couplings of Table VII. Finally, diagrams (6a) and (6b) depends on the FFS and FFV couplings of Table IV, as well as on the charged-current FFS and FFV interactions with SM and exotic quarks of Table VIII. The latter are proportional to the SM and exotic CKM matrices V_{CKM} and V'_{CKM} driving the mixing of the SM down-type quarks and exotic quarks, respectively.

Interaction	Coupling
$W_L^+ W_L^- h$	$i\frac{g_L^2}{2}[kU_{11}^H + v_L U_{21}^H]$
$W_L^+ W_L^- H_2^0$	$i\frac{g_L^2}{2}[kU_{12}^H + v_L U_{22}^H]$
$W_L^+ W_L^- H_3^0$	$i\frac{g_{L,R}^2}{2}[kU_{13}^H + v_L U_{23}^H]$
$W_L^+ W_L^- A_2^0$	0
$W_R^+ W_R^- h$	$i\frac{g_R^2}{2}[kU_{11}^H + v_R U_{31}^H]$
$W_R^+ W_R^- H_2^0$	$i\frac{g_R^2}{2}[kU_{12}^H + v_R U_{32}^H]$
$W_R^+ W_R^- H_3^0$	$i\frac{g_R^2}{2}[kU_{13}^H + v_R U_{33}^H]$
$W_R^+ W_R^- A_2^0$	0

Interaction	Couplings
$W_L^- H_1^+ h$	$-i\frac{g_L}{4}\frac{v_L U_{11}^H + kU_{21}^H}{\sqrt{k^2+v_L^2}}$
$W_L^- H_1^+ H_2^0$	$-i\frac{g_L}{4}\frac{v_L U_{12}^H + kU_{22}^H}{\sqrt{k^2+v_L^2}}$
$W_L^- H_1^+ H_3^0$	$-i\frac{g_L}{4}\frac{v_L U_{13}^H + kU_{23}^H}{\sqrt{k^2+v_L^2}}$
$W_L^- H_1^+ A_2^0$	$\frac{g_L}{\sqrt{2}}U_{22}^A$
$W_R^- H_2^+ h$	$-i\frac{g_R}{2}\frac{v_R U_{11}^H - kU_{31}^H}{\sqrt{k^2+v_R^2}}$
$W_R^- H_2^+ H_2^0$	$-i\frac{g_R}{2}\frac{v_R U_{12}^H - kU_{32}^H}{\sqrt{k^2+v_R^2}}$
$W_R^- H_2^+ H_3^0$	$-i\frac{g_R}{2}\frac{v_R U_{13}^H - kU_{33}^H}{\sqrt{k^2+v_R^2}}$
$W_R^- H_2^+ A_2^0$	$-\frac{g_R}{\sqrt{2}}U_{22}^A$

TABLE VII: VVS and SSV couplings appearing in the two-loop contributions to Δa_μ.

Interaction	Scalar (g_S)	Pseudo-scalar (g_P)	Interaction	Vector (g_V)	Axial-vector (g_A)
$\bar{t}bH_1^+$	$\frac{i}{2}(V_{\text{CKM}}^*)_{33}\dfrac{v_L Y_{33}^q + kY_{L,33}^q}{\sqrt{k^2+v_L^2}}$	$-\frac{i}{2}(V_{\text{CKM}}^*)_{33}\dfrac{v_L Y_{33}^q - kY_{L,33}^q}{\sqrt{k^2+v_L^2}}$	$\bar{t}bW_L^+$	$i\frac{g_L}{2\sqrt{2}}(V_{\text{CKM}}^*)_{33}$	$-i\frac{g_L}{2\sqrt{2}}(V_{\text{CKM}}^*)_{33}$
$\bar{t}q'_{d,i}H_2^+$	$\frac{i}{2}(V'^*_{\text{CKM}})_{3i}\dfrac{v_R Y_t + kY_{R,ii}^q}{\sqrt{k^2+v_R^2}}$	$-\frac{i}{2}(V'^*_{\text{CKM}})_{31}\dfrac{v_R Y_{33}^q - kY_{R,ii}^q}{\sqrt{k^2+v_R^2}}$	$\bar{t}q'_{d,i}W_R^+$	$i\frac{g_R}{2\sqrt{2}}(V'^*_{\text{CKM}})_{3i}$	$i\frac{g_R}{2\sqrt{2}}(V'^*_{\text{CKM}})_{3i}$

TABLE VIII: Charged-current FFV and FFS couplings appearing in the two-loop contributions to Δa_μ of diagrams (6a) and (6b) in Fig. 4, split in their scalar/vector and pseudo-scalar/axial-vector components. The index i is a generation index.

[1] J. C. Pati and A. Salam, "Lepton Number as the Fourth Color," *Phys. Rev.* **D10** (1974) 275–289. [Erratum: Phys. Rev.D11,703(1975)].

[2] R. Mohapatra and J. C. Pati, "A Natural Left-Right Symmetry," *Phys.Rev.* **D11** (1975) 2558.

[3] G. Senjanovic and R. N. Mohapatra, "Exact Left-Right Symmetry and Spontaneous Violation of Parity," *Phys. Rev.* **D12** (1975) 1502.

[4] R. N. Mohapatra, F. E. Paige, and D. Sidhu, "Symmetry Breaking and Naturalness of Parity Conservation in Weak Neutral Currents in Left-Right Symmetric Gauge Theories," *Phys.Rev.* **D17** (1978) 2462.

[5] F. Gursey, P. Ramond, and P. Sikivie, "A Universal Gauge Theory Model Based on E6," *Phys. Lett.* **60B** (1976) 177–180.

[6] Y. Achiman and B. Stech, "Quark Lepton Symmetry and Mass Scales in an E6 Unified Gauge Model," *Phys. Lett.* **77B** (1978) 389–393.

[7] J. L. Hewett and T. G. Rizzo, "Low-Energy Phenomenology of Superstring Inspired E(6) Models," *Phys. Rept.* **183** (1989) 193.

[8] E. Ma, "Particle Dichotomy and Left-Right Decomposition of E(6) Superstring Models," *Phys. Rev.* **D36** (1987) 274.

[9] K. Babu, X.-G. He, and E. Ma, "New Supersymmetric Left-Right Gauge Model: Higgs Boson Structure and Neutral Current Analysis," *Phys.Rev.* **D36** (1987) 878.

[10] M. Frank, I. Turan, and M. Sher, "Neutrino masses in the effective rank-5 subgroups of E(6): Supersymmetric case," *Phys. Rev.* **D71** (2005) 113002, [hep-ph/0503084].

[11] E. Ma, "Dark Left-Right Model: CDMS, LHC, etc.," *J.Phys.Conf.Ser.* **315** (2011) 012006, [1006.3804].

[12] M. Ashry and S. Khalil, "Phenomenological aspects of a TeV-scale alternative left-right model," *Phys. Rev. D* **91** no. 1, (2015) 015009, [1310.3315]. [Addendum: Phys.Rev.D 96, 059901 (2017)].

[13] M. Frank, I. Turan, and M. Sher, "Neutrino masses in effective rank-5 subgroups of e(6) I: Non-SUSY case," *Phys. Rev.* **D71** (2005) 113001, [hep-ph/0412090].

[14] M. Frank, B. Fuks, and O. Özdal, "Natural dark matter and light bosons with an alternative left-right symmetry," *JHEP* **04** (2020) 116, [1911.12883].

[15] M. Frank, C. Majumdar, P. Poulose, S. Senapati, and U. A. Yajnik, "Dark matter in the Alternative Left Right model," *JHEP* **12** (2022) 032, [2211.04286].

[16] **ATLAS** Collaboration, G. Aad *et al.*, "Search for high-mass dilepton resonances using 139 fb^{-1} of pp collision data collected at $\sqrt{s}$ =13 TeV with the ATLAS detector," *Phys. Lett. B* **796** (2019) 68–87, [1903.06248].

[17] **CMS** Collaboration, A. M. Sirunyan *et al.*, "Search for resonant and nonresonant new phenomena in high-mass dilepton final states at $\sqrt{s}$ = 13 TeV," *JHEP* **07** (2021) 208, [2103.02708].

[18] M. Frank, C. Majumdar, P. Poulose, S. Senapati, and U. A. Yajnik, "Vacuum structure of Alternative Left-Right Model," *JHEP* **03** (2022) 065, [2111.08582].

[19] M. Frank, C. Majumdar, P. Poulose, S. Senapati, and U. A. Yajnik, "Exploring $0\nu\beta\beta$ and leptogenesis in the alternative left-right model," *Phys. Rev. D* **102** no. 7, (2020) 075020, [2008.12270].

[20] M. Frank, B. Fuks, S. K. Garg, and P. Poulose, "Flavour-changing top quark decays in the alternative left-right model," *Phys. Lett. B* **850** (2024) 138548, [2312.12523].

[21] A. Czarnecki, W. J. Marciano, and A. Vainshtein, "Refinements in electroweak contributions to the muon anomalous magnetic moment," *Phys. Rev. D* **67** (2003) 073006, [hep-ph/0212229]. [Erratum: Phys.Rev.D 73, 119901 (2006)].

[22] K. Melnikov and A. Vainshtein, "Hadronic light-by-light scattering contribution to the muon anomalous magnetic moment revisited," *Phys. Rev. D* **70** (2004) 113006, [hep-ph/0312226].

[23] T. Aoyama, M. Hayakawa, T. Kinoshita, and M. Nio, "Complete Tenth-Order QED Contribution to the Muon g-2," *Phys. Rev. Lett.* **109** (2012) 111808, [1205.5370].

[24] C. Gnendiger, D. Stöckinger, and H. Stöckinger-Kim, "The electroweak contributions to $(g-2)_\mu$ after the Higgs boson mass measurement," *Phys. Rev. D* **88** (2013) 053005, [1306.5546].

[25] G. Colangelo, M. Hoferichter, A. Nyffeler, M. Passera, and P. Stoffer, "Remarks on higher-order hadronic corrections to the muon g−2," *Phys. Lett. B* **735** (2014) 90–91, [1403.7512].

[26] A. Kurz, T. Liu, P. Marquard, and M. Steinhauser, "Hadronic contribution to the muon anomalous magnetic moment to next-to-next-to-leading order," *Phys. Lett. B* **734** (2014) 144–147, [1403.6400].

[27] P. Masjuan and P. Sanchez-Puertas, "Pseudoscalar-pole contribution to the $(g_\mu - 2)$: a rational approach," *Phys. Rev. D* **95** no. 5, (2017) 054026, [1701.05829].

[28] G. Colangelo, M. Hoferichter, M. Procura, and P. Stoffer, "Dispersion relation for hadronic light-by-light scattering: two-pion contributions," *JHEP* **04** (2017) 161, [1702.07347].

[29] A. Keshavarzi, D. Nomura, and T. Teubner, "Muon $g - 2$ and $\alpha(M_Z^2)$: a new data-based analysis," *Phys. Rev. D* **97** no. 11, (2018) 114025, [1802.02995].

[30] G. Colangelo, M. Hoferichter, and P. Stoffer, "Two-pion contribution to hadronic vacuum polarization," *JHEP* **02** (2019) 006, [1810.00007].

[31] M. Hoferichter, B.-L. Hoid, B. Kubis, S. Leupold, and S. P. Schneider, "Dispersion relation for hadronic light-by-light scattering: pion pole," *JHEP* **10** (2018) 141, [1808.04823].

[32] J. Bijnens, N. Hermansson-Truedsson, and A. Rodríguez-Sánchez, "Short-distance constraints for the HLbL contribution to the muon anomalous magnetic moment," *Phys. Lett. B* **798** (2019) 134994, [1908.03331].

[33] T. Blum, N. Christ, M. Hayakawa, T. Izubuchi, L. Jin, C. Jung, and C. Lehner, "Hadronic Light-by-Light Scattering Contribution to the Muon Anomalous Magnetic Moment from Lattice QCD," *Phys. Rev. Lett.* **124** no. 13, (2020) 132002, [1911.08123].

[34] G. Colangelo, F. Hagelstein, M. Hoferichter, L. Laub, and P. Stoffer, "Longitudinal short-distance constraints for the hadronic light-by-light contribution to $(g-2)_\mu$ with large-N_c Regge models," *JHEP* **03** (2020) 101, [1910.13432].

[35] M. Hoferichter, B.-L. Hoid, and B. Kubis, "Three-pion contribution to hadronic vacuum polarization," *JHEP* **08** (2019) 137, [1907.01556].

[36] A. Gérardin, H. B. Meyer, and A. Nyffeler, "Lattice calculation of the pion transition form factor with $N_f = 2 + 1$ Wilson quarks," *Phys. Rev. D* **100** no. 3, (2019) 034520, [1903.09471].

[37] A. Keshavarzi, D. Nomura, and T. Teubner, "$g - 2$ of charged leptons, $\alpha(M_Z^2)$, and the hyperfine splitting of muonium," *Phys. Rev. D* **101** no. 1, (2020) 014029, [1911.00367].

[38] T. Aoyama *et al.*, "The anomalous magnetic moment of the muon in the Standard Model," *Phys. Rept.* **887** (2020) 1–166, [2006.04822].

[39] **Muon g-2** Collaboration, J. Grange *et al.*, "Muon (g-2) Technical Design Report," [1501.06858].

[40] **Muon g-2** Collaboration, T. Albahri *et al.*, "Measurement of the anomalous precession frequency of the muon in the Fermilab Muon $g - 2$ Experiment," *Phys. Rev. D* **103** no. 7, (2021) 072002, [2104.03247].

[41] **Muon g-2** Collaboration, B. Abi *et al.*, "Measurement of the Positive Muon Anomalous Magnetic Moment to 0.46 ppm," *Phys. Rev. Lett.* **126** no. 14, (2021) 141801, [2104.03281].

[42] S. Borsanyi *et al.*, "Leading hadronic contribution to the muon magnetic moment from lattice QCD," *Nature* **593** no. 7857, (2021) 51–55, [2002.12347].

[43] M. Cè *et al.*, "Window observable for the hadronic vacuum polarization contribution to the muon g-2 from lattice QCD," *Phys. Rev. D* **106** no. 11, (2022) 114502, [2206.06582].

[44] **Extended Twisted Mass** Collaboration, C. Alexandrou *et al.*, "Lattice calculation of the short and intermediate time-distance hadronic vacuum polarization contributions to the muon magnetic moment using twisted-mass fermions," *Phys. Rev. D* **107** no. 7, (2023) 074506, [2206.15084].

[45] **RBC, UKQCD** Collaboration, T. Blum *et al.*, "Update of Euclidean windows of the hadronic vacuum polarization," *Phys. Rev. D* **108** no. 5, (2023) 054507, [2301.08696].

[46] **Fermilab Lattice, HPQCD,, MILC** Collaboration, A. Bazavov *et al.*, "Light-quark connected intermediate-window contributions to the muon g-2 hadronic vacuum polarization from lattice QCD," *Phys. Rev. D* **107** no. 11, (2023) 114514, [2301.08274].

[47] H. Wittig, "Progress on $(g - 2)_\mu$ from Lattice QCD," in *57th Rencontres de Moriond on Electroweak Interactions and Unified Theories.* 6, 2023. [2306.04165].

[48] S. J. Brodsky and J. D. Sullivan, "W BOSON CONTRIBUTION TO THE ANOMALOUS MAGNETIC MOMENT OF THE MUON," *Phys. Rev.* **156** (1967) 1644–1647.

[49] T. Burnett and M. J. Levine, "Intermediate vector boson contribution to the muon's anomalous magnetic moment," *Phys. Lett. B* **24** (1967) 467–468.

[50] R. Jackiw and S. Weinberg, "Weak interaction corrections to the muon magnetic moment and to muonic atom energy levels," *Phys. Rev. D* **5** (1972) 2396–2398.

[51] I. Bars and M. Yoshimura, "Muon magnetic moment in a finite theory of weak and electromagnetic interaction," *Phys. Rev. D* **6** (1972) 374–376.

[52] K. Fujikawa, B. W. Lee, and A. I. Sanda, "Generalized Renormalizable Gauge Formulation of Spontaneously Broken Gauge Theories," *Phys. Rev. D* **6** (1972) 2923–2943.

[53] G. Altarelli, N. Cabibbo, and L. Maiani, "The Drell-Hearn sum rule and the lepton magnetic moment in the Weinberg model of weak and electromagnetic interactions," *Phys. Lett. B* **40** (1972) 415–419.

[54] W. A. Bardeen, R. Gastmans, and B. E. Lautrup, "Static quantities in Weinberg's model of weak and electromagnetic interactions," *Nucl. Phys. B* **46** (1972) 319–331.

[55] M. Lindner, M. Platscher, and F. S. Queiroz, "A Call for New Physics : The Muon Anomalous Magnetic Moment and Lepton Flavor Violation," *Phys. Rept.* **731** (2018) 1–82, [1610.06587].

[56] B. Yu and S. Zhou, "General remarks on the one-loop contributions to the muon anomalous magnetic moment," *Nucl. Phys. B* **975** (2022) 115674, [2106.11291].

[57] J. P. Leveille, "The Second Order Weak Correction to (G-2) of the Muon in Arbitrary Gauge Models," *Nucl. Phys. B* **137** (1978) 63–76.

[58] W. Altmannshofer, C.-Y. Chen, P. S. Bhupal Dev, and A. Soni, "Lepton flavor violating Z′ explanation of the muon anomalous magnetic moment," *Phys. Lett. B* **762** (2016) 389–398, [1607.06832].

[59] S. N. Gninenko and N. V. Krasnikov, "The Muon anomalous magnetic moment and a new light gauge boson," *Phys.*

Lett. B **513** (2001) 119, [`hep-ph/0102222`].

[60] S. Jana, V. P. K., and S. Saad, "Resolving electron and muon $g - 2$ within the 2HDM," *Phys. Rev. D* **101** no. 11, (2020) 115037, [`2003.03386`].

[61] M. Krawczyk and J. Zochowski, "Constraining 2HDM by present and future muon (g-2) data," *Phys. Rev. D* **55** (1997) 6968–6974, [`hep-ph/9608321`].

[62] F. Larios, G. Tavares-Velasco, and C. P. Yuan, "A Very light CP odd scalar in the two Higgs doublet model," *Phys. Rev. D* **64** (2001) 055004, [`hep-ph/0103292`].

[63] A. Dedes and H. E. Haber, "Can the Higgs sector contribute significantly to the muon anomalous magnetic moment?," *JHEP* **05** (2001) 006, [`hep-ph/0102297`].

[64] F. S. Queiroz and W. Shepherd, "New Physics Contributions to the Muon Anomalous Magnetic Moment: A Numerical Code," *Phys. Rev. D* **89** no. 9, (2014) 095024, [`1403.2309`].

[65] A. Broggio, E. J. Chun, M. Passera, K. M. Patel, and S. K. Vempati, "Limiting two-Higgs-doublet models," *JHEP* **11** (2014) 058, [`1409.3199`].

[66] M. C. Gonzalez-Garcia, M. Maltoni, and T. Schwetz, "NuFIT: Three-Flavour Global Analyses of Neutrino Oscillation Experiments," *Universe* **7** no. 12, (2021) 459, [`2111.03086`].

[67] J. D. Bjorken and S. Weinberg, "A Mechanism for Nonconservation of Muon Number," *Phys. Rev. Lett.* **38** (1977) 622.

[68] S. M. Barr and A. Zee, "Electric Dipole Moment of the Electron and of the Neutron," *Phys. Rev. Lett.* **65** (1990) 21–24. [Erratum: Phys.Rev.Lett. 65, 2920 (1990)].

[69] D. Chang, W.-F. Chang, C.-H. Chou, and W.-Y. Keung, "Large two loop contributions to g-2 from a generic pseudoscalar boson," *Phys. Rev. D* **63** (2001) 091301, [`hep-ph/0009292`].

[70] J. F. Gunion, "A Light CP-odd Higgs boson and the muon anomalous magnetic moment," *JHEP* **08** (2009) 032, [`0808.2509`].

[71] L. Wang and X.-F. Han, "A light pseudoscalar of 2HDM confronted with muon g-2 and experimental constraints," *JHEP* **05** (2015) 039, [`1412.4874`].

[72] V. Ilisie, "New Barr-Zee contributions to $(\mathbf{g} - \mathbf{2})_\mu$ in two-Higgs-doublet models," *JHEP* **04** (2015) 077, [`1502.04199`].

[73] **MEG II** Collaboration, M. Chiappini, "MEG II physics and detector performance," *JINST* **18** no. 10, (2023) C10020.

[74] A. M. Baldini *et al.*, "MEG Upgrade Proposal," [`1301.7225`].

[75] **SINDRUM II** Collaboration, W. H. Bertl *et al.*, "A Search for muon to electron conversion in muonic gold," *Eur. Phys. J. C* **47** (2006) 337–346.

[76] **SINDRUM II** Collaboration, P. Wintz *et al.*, "Test of LFC in mu —> e conversion on titanium," in *14th International Conference on Particles and Nuclei*, pp. 458–459. 5, 1996.

[77] **Mu2e** Collaboration, G. Pezzullo, "The Mu2e experiment at Fermilab: a search for lepton flavor violation," *Nucl. Part. Phys. Proc.* **285-286** (2017) 3–7, [`1705.06461`].

[78] A. Ilakovac and A. Pilaftsis, "Flavor violating charged lepton decays in seesaw-type models," *Nucl. Phys. B* **437** (1995) 491, [`hep-ph/9403398`].

[79] F. Deppisch and J. W. F. Valle, "Enhanced lepton flavor violation in the supersymmetric inverse seesaw model," *Phys. Rev. D* **72** (2005) 036001, [`hep-ph/0406040`].

[80] F. Deppisch, T. S. Kosmas, and J. W. F. Valle, "Enhanced mu- - e- conversion in nuclei in the inverse seesaw model," *Nucl. Phys. B* **752** (2006) 80–92, [`hep-ph/0512360`].

[81] A. Ilakovac and A. Pilaftsis, "Supersymmetric Lepton Flavour Violation in Low-Scale Seesaw Models," *Phys. Rev. D* **80** (2009) 091902, [`0904.2381`].

[82] R. Alonso, M. Dhen, M. B. Gavela, and T. Hambye, "Muon conversion to electron in nuclei in type-I seesaw models," *JHEP* **01** (2013) 118, [`1209.2679`].

[83] D. N. Dinh, A. Ibarra, E. Molinaro, and S. T. Petcov, "The $\mu - e$ Conversion in Nuclei, $\mu \to e\gamma, \mu \to 3e$ Decays and TeV Scale See-Saw Scenarios of Neutrino Mass Generation," *JHEP* **08** (2012) 125, [`1205.4671`]. [Erratum: JHEP 09, 023 (2013)].

[84] A. Ilakovac, A. Pilaftsis, and L. Popov, "Charged lepton flavor violation in supersymmetric low-scale seesaw models," *Phys. Rev. D* **87** no. 5, (2013) 053014, [`1212.5939`].

[85] A. Abada, D. Das, A. Vicente, and C. Weiland, "Enhancing lepton flavour violation in the supersymmetric inverse seesaw beyond the dipole contribution," *JHEP* **09** (2012) 015, [`1206.6497`].

[86] C.-H. Lee, P. S. Bhupal Dev, and R. N. Mohapatra, "Natural TeV-scale left-right seesaw mechanism for neutrinos and experimental tests," *Phys. Rev. D* **88** no. 9, (2013) 093010, [`1309.0774`].

[87] S. Weinberg and G. Feinberg, "Electromagnetic Transitions Between mu Meson and Electron," *Phys. Rev. Lett.* **3** (1959) 111–114.

[88] W. J. Marciano and A. I. Sanda, "The Reaction mu- Nucleus –> e- Nucleus in Gauge Theories," *Phys. Rev. Lett.* **38** (1977) 1512.

[89] A. Czarnecki, W. J. Marciano, and K. Melnikov, "Coherent muon electron conversion in muonic atoms," *AIP Conf. Proc.* **435** no. 1, (1998) 409–418, [`hep-ph/9801218`].

[90] R. Kitano, M. Koike, and Y. Okada, "Detailed calculation of lepton flavor violating muon electron conversion rate for various nuclei," *Phys. Rev. D* **66** (2002) 096002, [`hep-ph/0203110`]. [Erratum: Phys.Rev.D 76, 059902 (2007)].

[91] V. Cirigliano, A. Kurylov, M. J. Ramsey-Musolf, and P. Vogel, "Lepton flavor violation without supersymmetry," *Phys. Rev. D* **70** (2004) 075007, [`hep-ph/0404233`].

[92] V. Cirigliano, R. Kitano, Y. Okada, and P. Tuzon, "On the model discriminating power of mu —> e conversion in nuclei," *Phys. Rev. D* **80** (2009) 013002, [`0904.0957`].

[93] L. Borrel, D. G. Hitlin, and S. Middleton, "A New Determination of the (Z,A) Dependence of Coherent

Muon-to-Electron Conversion," [2401.15025].

[94] W. C. Haxton and E. Rule, "Distinguishing charged lepton flavor violation scenarios with inelastic $\mu \to e$ conversion," [2404.17166].

[95] W. Haxton, K. McElvain, T. Menzo, E. Rule, and J. Zupan, "Effective theory tower for $\mu \to e$ conversion," [2406.13818].

[96] **DeeMe** Collaboration, H. Natori, "An experiment to search for mu-e conversion at J-PARC MLF in Japan, DeeMe experiment," *PoS* **ICHEP2018** (2019) 642.

[97] **Mu2e** Collaboration, S. Di Falco, "The Mu2e experiment," *PoS* **EPS-HEP2023** (2024) 461.

[98] **COMET** Collaboration, Y. Fujii, "A search for a muon to electron conversion in COMET," *JINST* **18** no. 10, (2023) C10010, [2308.14275].

[99] Y. Kuno and Y. Okada, "Mu —> e gamma search with polarized muons," *Phys. Rev. Lett.* **77** (1996) 434–438, [hep-ph/9604296].

[100] A. Crivellin, S. Davidson, G. M. Pruna, and A. Signer, "Renormalisation-group improved analysis of $\mu \to e$ processes in a systematic effective-field-theory approach," *JHEP* **05** (2017) 117, [1702.03020].

[101] A. Crivellin, M. Hoferichter, and M. Procura, "Improved predictions for $\mu \to e$ conversion in nuclei and Higgs-induced lepton flavor violation," *Phys. Rev. D* **89** (2014) 093024, [1404.7134].

[102] J. Heeck, R. Szafron, and Y. Uesaka, "Isotope dependence of muon-to-electron conversion," *Nucl. Phys. B* **980** (2022) 115833, [2203.00702].

[103] T. Suzuki, D. F. Measday, and J. P. Roalsvig, "Total Nuclear Capture Rates for Negative Muons," *Phys. Rev. C* **35** (1987) 2212.

[104] P. Fileviez Perez and C. Murgui, "Lepton Flavour Violation in Left-Right Theory," *Phys. Rev. D* **95** no. 7, (2017) 075010, [1701.06801].